2014

Time-resolved investigation of fast pyrolysis using FTIR spectroscopy

Nandith George Chandy
Iowa State University

Time-resolved investigation of fast pyrolysis using FTIR spectroscopy

by

Nandith George Chandy

A thesis submitted to the graduate faculty

in partial fulfillment of the requirements for the degree of

MASTER OF SCIENCE

Major: Mechanical Engineering

Program of Study Committee:
Terrence Meyer, Major Professor

Mark Mba Wright

Brent Shanks

Iowa State University

Ames, Iowa

2014

TABLE OF CONTENTS

Page

LIST OF FIGURES

Page

ACKNOWLEDGEMENTS

I would like to take this opportunity to thank my Major Professor Dr. Terrence Meyer for giving me this opportunity to work on something so novel and interesting. I would also like to thank my committee members, Dr. Mark MBA Wright and Dr. Brent Shanks. I have had the privilege to work with and get valuable insight from my lab mates, Jordan Tiarks, Eric Chon, Patrick Sanderson, Chloe Dedic, James Michael, Prabhakar Venkateswaran, and Harish Subramani. Their help with experimental techniques and data management have been very helpful. I would like to specially thank Nitya Poovaiah for her help in making me understand a lot of the Chemisrty in the present work. I would like to thank Professor Chien Peng of the Applied Sciences Department for being very patient about my work. Willem Lubberden was very helpful in giving me tips on the research after I had taken an internship hiatus, and it was wonderful working with him in the early stages of the research. I would also like to thank Patrick Johnston of the BRL for taking the time to teach and provide valuable information on the research. The Mechanical Engineering Department has also been very helpful by providing a positive and stress free environment to work in. None of this would be possible without the support of my family, their support has been a great influence in my work and I would like to dedicate this thesis to them. My friends have always been with me to cheer me up through the tough days and I am very grateful to them. I would also like to thank my Brazilian Jiu Jitsu coach for giving me an outlet to work on improving myself as a person. I would also like to thank God for this amazing opportunity and this journey that has been given to me.

ABSTRACT

A bench scale pyrolysis reactor was developed to study the evolutions of species during the pyrolysis of biomass and for different product residence times. The product residence times were controlled by the flow rate of sweep gas inside of the reactor. Two product residence times of 0.9 and 1.4 seconds were studied. The reactor has optical access which allows for *in-situ* diagnosis of the products in the reactor. In this study, Fourier Transform Infrared Spectroscopy (FTIR) was adapted to allow for the I.R. beam to be drawn out of the standard sample chamber for propagation through the pyrolysis reactor and subsequent spectral analysis. The *in-situ* FTIR spectra allowed for time-resolved studies of the product evolution during pyrolysis. The two biomass substances that were studied were cellulose and lignin. Their evolution trends were studied and reported as well as the approximate evolution times for certain species classified by bond groups. The data reported shows that the methods established in this work can be used for temperal analysis of pyrolysis for various feedstocks and test conditions, potentially helping to improve the understanding of the kinetics of biomass fast pyrolysis.

CHAPTER 1. INTRODUCTION

1.1 Motivation

Because of the growth in population and industrialization throughout the world, the demand for reliable sources of energy is constantly increasing. According to the world energy council the world is facing an energy trilemma. The requirement of energy is has three major effecting factors, energy equity, energy security and environmental sustainability [1]. Energy equity refers to the affordability and accessibility of energy. Energy security is the ability to provide energy now and in the future. Energy sustainability refers to the development of energy supplies from renewable sources. The development of biofuels from biomass serves as one method to solve the trilemma It helps improve affordability of fuels by reducing the dependence on outside countries. There is security assured when land is cultivated to support biofuel production, and it is a renewable source of energy which helps sustainability. Fuels such as biodiesel have lower greenhouse gas emissions compared to conventional fuels as well as lower prices. The United States department of energy fuel price report as of July 2014 shows that ethanol is priced at $3.41 per gallon as compared to regular gasoline at $3.65 per gallon [2]. Therefore there are monetary as well as environmental gains in biofuel use.

The thermochemical upgrading to biofuels first requires the production of bio-oil. Bio-oil can be produced by the thermal decomposition of biomass in the absence of oxygen, aka Pyrolysis. It has been found that the production of bio-oils via fast pyrolysis reaches a maximum at temperatures ranging from 400 – 550^{o}C [3]. This temperature range

typically yields 60-75 wt% of liquid bio-oil [4]. Many studies have been conducted on fast pyrolysis but there are no studies that give a good kinetic understanding of the fast pyrolysis process. This served as the main motivation for this thesis. A reactor was fabricated to allow for the *in-situ* time-evolution studies of fast pyrolysis so that reaction kinetics could be studied with optical diagnostics. This thesis focuses on the utilization of Fourier Transform Infrared Spectroscopy (FTIR) and establishes the methods and tools that can be used to obtain a better understanding of fast pyrolysis temporal characteristics.

1.2 Objective

The objective of this study is to first develop a fast pyrolysis reactor with optical access to allow for *in-situ* diagnosis of the pyrolysis process. The reactor can then need to be characterized based on the requirements of fast pyrolysis. This includes reaction temperatures, particle sizes, and product residence times. The temporal evolution characteristics of the products during the reactions will be studied using Fourier Transform Infrared Spectroscopy (FTIR). Through these tests inferences can be obtained on the evolution times of a wide range of species characterized by detected bond groups.

CHAPTER 2. LITERATURE REVIEW

2.1 Composition of Biomass

Biomass is one of the oldest sources of energy in the world and has been a modern source of alternative energy since the 1970's [5]. Given limited energy supplies at various points in recent history and inevitably in the future, it is attractive as an ecofriendly renewable source of energy. The chemical composition of biomass shows large amounts of oxygen present, which differentiates biomass sharply from other fossil fuels. The major components in biomass are carbohydrate polymers and oligomers (65%-75%) and lignin (18%-35%) [6]. The major constituents with varying weights in different biomass types include, Cellulose, Hemicellulose, and Lignin [6]. Hence, the pyrolysis of these compounds are of interest in the current study.

2.1.1 Cellulose

Cellulose fibers make up roughly 40-50 wt% of dry wood. It is an insoluble crystalline material consisting of long chains that are bound by hydrogen bonds. Microfibril sheets that make up a variety of complex fibres in trees are made from cellulose chains [6]. Due to its crystalline structure cellulose resists thermal decomposition better than hemicellulose. Pyrolysis of cellulose at lower temperature $<300^{o}C$ favors the formation of char and gas whereas at higher temperatures a tarry pyrolyzate containing a 22-50% of Levoglucosan is formed, which vaporizes at higher temperatures [7].

2.1.2 Hemicellulose

Hemicellulose aka polyose is the second major component of biomass with weight percentages varying from 25-35%. It is a mixture of polymerized monomers like glucose, mannose, galactose, xylose, arabinose, 4-O-methyl glucuronic acid and galacturonic acid residues [6]. Compared to Cellulose, hemicellulose has a lower molecular weight and has a heteropolysacharide makeup. Hemicellulose is the most reactive major component of biomass and begins its decomposition at a range of 200-260^{o}C. During pyrolysis hemicellulose produces more gases, methanol and acetic acid than does cellulose. It also produces less tar compared to cellulose [7].

2.1.3 Lignin

The third major component in woody biomass is Lignin. It can be thought of the cement that binds together the cellulose micro fibrils. Lignin is the least reactive of the components of biomass and decomposes at higher temperatures (280-500^{o}C) [7]. To obtain lignin, isolation technology is required. These change the chemical and physical properties of the lignin. Therefore, the products of thermal decomposition of lignin may not be the same as the component found in the original biomass [6]. Here we utilized pure lignin as a test case, although future studies can include whole biomass.

2.1.4 Inorganic Materials

Inorganic materials usually comprise the ash content in biomass. They also contain various metal cations of which the majority is K and Ca, with the remaining being Na, P

and Mg [8]. Metal cations have effects on pyrolysis products which include the lowering of tar yields due to their reactive nature.

2.2 Pyrolysis

The etymology of Pyrolysis is derived from the Greek word ‘Pûr’ translating to fire and ‘Lúsis’ translating to loosing. From the translation one can infer that pyrolysis is the thermal decomposition of material in the absence of oxygen, therefore no fire is generated. This procedure leads to the evolution of liquids, gases and solid residue called char [7,4,6]. Oil is a nonrenewable source of fuel today. In a world of growing economies such as the nations of Brazil, Russia, India and China (BRIC), the need for different sources of fuel is very apparent. The utilization of biomass pyrolysis for energy provides environmental advantages. Growth of biomass plats for feedstock reduces the amount of carbon dioxide in the atmosphere; this offsets the amount of carbon dioxide released by bio fuel combustion [6]

Biomass pyrolysis can be split up into 4 stages.

1. Moisture evolution.
2. Hemicellulose decomposition
3. Cellulose decomposition
4. Lignin decomposition [9]

Rapid heating of the biomass causes the breakdown of the carbohydrates into volatile, low molecular weight compounds. Char formation occurs mainly when there are higher

product residence times and low heating rates. As a rule the following simple species evolve from pyrolysis of most organics: CH_4, C_2H_4, CO_2, CO, H_2O, NH_3, HCN, SO_2 and COS [10].

2.2.1 Types of Pyrolysis

1. Slow pyrolysis: Slow pyrolysis is characterized by low heating rates and thus longer residence times. Heating rates are subjective to the system and may vary from 0.1 to 2^{o}C per second at temperatures of 500^{o}C. Since the residence times are long the primary products undergo secondary reactions. The volatiles have enough time to escape and thus the main products are tar and char. This is due to re-polymerization and recombination reactions [7].
2. Fast pyrolysis: Fast pyrolysis can readily produce a liquid fuel from biomass [7]**.** The residence times are shorter and the heating rates are much higher compared to slow pyrolysis. The usual heating rates are 10-1000^{o}C/s and the reactor temperatures are above 500^{o}C. The products are high-quality ethylene rich gases that can be used to create alcohols and gasoline as well as aerosols and charcoal [7,6]. For liquid production very low residence times of the order of 1s are required as well as small particle size [11,7,6,12]. For the generation of bio oil rapid cooling of the pyrolysis products is important. Bio-oil is important to study because it has a density of 1200 kg/m^3, which is higher than fuel oil and has a 42% energy content of fuel based on weight [7]. For the production of bio-oils to be used as fuels, longer product residence times can be used (up to 5 s). [6]. Pushkaraj et al. states that bio-oils are a complex mixture of many compounds

classified as low molecular weight compounds, furan pyran ring derivatives, phenolic compounds, and anhydro sugars [13]. An example of a fast pyrolysis reactor is given in Fig. 1 taken directly from Ref. [14].

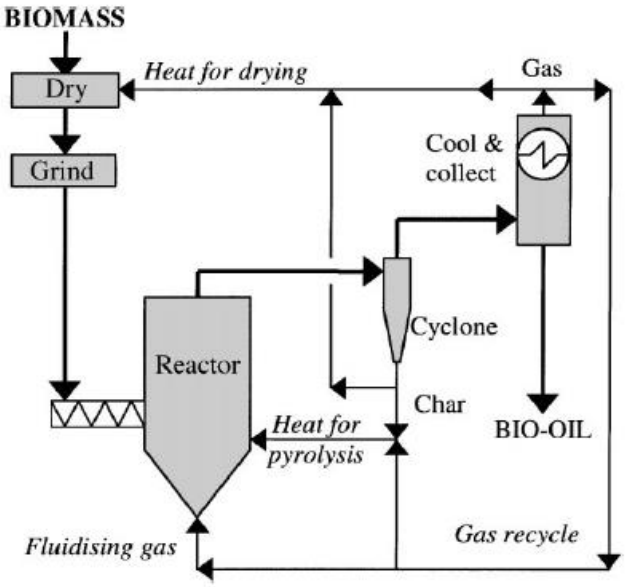

Figure 1. Conceptual Fluidized bed reactor [14].

3. Flash pyrolysis: Flash pyrolysis prevailing temperatures are between 1050 – 1300 K and the heating rates are greater than 1000 K/s. The particle sizes are less than 0.2 mm and the solid residence times are less than 0.5 s [12,7].

2.2.2 Factors Affecting Pyrolysis

Biomass Pyrolysis is greatly affected by the following factors:

1. Substrate composition: The main components of biomass are responsible for the complexity of the products formed. Biomass has a heterogeneous composition of hemicellulose, cellulose, and lignin. Above 300^{o}C hemicellulose and cellulose

break down to form char and tarry pyrolyzates, whereas lignin has a larger temperature range for its breakdown and leads to formation of more char and a lower amount of pyrolyzate [7]. The heterogeneity of biomass is a problem because the yields of individual products are low. This thereby affects the yield of charcoal and other types of fuel [7].

2. Feed preparation: There are particle limitations in biomass pyrolysis because of the heat transfer rates due to the fact that biomass is a poor heat conductor [11,3]. Pyrolysis of small particles occurs at high temperatures and high heating rates, whereas char formation is increased by pyrolysis of large particles, low temperatures, and low heating rates [7]. Moisture is generated in flash pyrolysis and bio-oil thus contains at least 15% water. This water affects the pH of the bio-oil and thus the corrosiveness of the oil and cannot be removed by conventional methods such as distillation. Selective condensation may reduce water content at the expense of low molecular weight volatile components [14]. High water content in biomass affects the calorific value of the biofuel--drying of the biomass is hence important and should be done thoroughly [5].

3. Heating rate: The heating rate in a pyrolysis reactor varies with different reactor types. Reactors such as the circulating fluid bed use both convection and conduction for heat transfer. The ablative reactor uses conduction for heat transfer [11] [6]. The heating rate is an important factor in biomass pyrolysis. This is due to the fact that the reactions have a large temperature range. Therefore, reactions happening at the beginning can undergo further

transformation with later reactions. Flash Pyrolysis is a method of reducing the secondary reactions. These reactions result in low amounts of char formation. The increase in volatile products is increased by higher heating rates [7,15]. This is because at high heating rates the volatiles do not have enough time to escape form the reaction zone.

Char and bio-oil are the main products that are seen at any temperature or heating rate. However, with faster heating rates the production of bio-oil is faster. Decomposition mainly occurs at temperatures below 500^0C. Salehi et al. reported that there was a big jump in the bio oil yields in changing heat transfer rates from 500-700^{o}C/min [16]. Sukiran et al similarly showed that bio-oil yields were maximum at 100^{o}C/min. compared to 10^{o}C/min [17].

4. Temperature: Increasing temperature rapidly causes the decrease in residence times and thus the formation of volatiles and low amounts of char. Bio-oil yields increase with the increase in the maximum temperature around $550^0 – 680^0$C and drops with further increase in temperature [7]. The total product yield is affected by temperature, reaching a maximum at 500-520^{o}C [14]. Gercel et al. while running fast pyrolysis tests on sunflower pressed bagasse showed that liquid oil yields were lower at 400^{o}C and 700^{o}C compared to 500^{o}C and 550^{o}C [18].

5. Catalysis: Impurities have a great influence on biomass pyrolysis reactions. The major impurities are trace inorganic compounds and metals. They can be inorganic additives or natural ash content. Ash content can lead to corrosion in

the reactor and cause agglomeration of pyrolyser bed materials [3]**.** Mineral matter decreases the amount of liquid oil yields and tends to increase the char and gas formation because they speed up dehydration and charring reactions during primary and secondary pyrolysis [3,19,15]. These catalysts have a high influence in cellulose reactions and very low effect on lignin reactions. Alkaline cations affect the thermal decomposition in fast pyrolysis and cause the fragmentation of the monomers that are in natural polymer chains [6] their presence in mineral matter enhances activity between alkali carbonates, -COOH and –OH functional groups forming alkali-oxygen clusters. Metal ions can be used to alter the products obtained by pyrolysis. K, Na, P, Ca and Mg are some of the metal cations present, of which Potassium and Calcium are a majority [8]. Metal cations are also responsible for low tar yields; this is due to the high catalytic reactivity of metal cations [3,20]. Acid catalysts catalyze the transglycosylation reactions [7]. They also help in enhancing the condensation of intermediate compounds.

6. Char Separation: Char is the dark residue formed in reactors during pyrolysis. It is formed by the devolatization of biomass during pyrolytic reactions [7]. Char can act as a vapor cracking catalyst and will affect the products of the pyrolysis reaction. Therefore, they must be removed from the reactor [5]. There are techniques that are employed in industry to curb the problem which includes filtration systems, particle separations, reducing the lignin content in the biomass and adding liquids and chemicals to reduce char formations.

7. Product residence time: It is accepted that for higher liquid yields, that shorter residence times are required [11,7,3]. At shorter residence times it is tough to conclude that all the biomass is being pyrolyzed because of the particle size. The residence times of the biomass must be longer than the product residence times from complete biomass conversion [21]. In order to optimize the product residence times for pyrolysis process one must consider the size of particles, type of bio-oil required, heating rates, complete biomass conversion, and sweeping of tars to prevent repolymerzation [3].

8. Particle feed size: Heat transfer in biomass is relatively poor. It is understood that for higher liquid yields the particle sizes should be smaller. This allows for the heat transfer assumption that the particle is being heated uniformly. Each pyrolysis reactor has different yields for different particle sizes. Aylon et al determined that using the same particle size of 2mm on a fixed bed and moving bed reactor gave different yields of liquid oils [22]. Sometimes, high yield of liquid is seen with larger particle sizes. This can be attributed to the presence of oxygen in the particle which may have a relationship to its heat transfer. Studies have shown that higher oxygen content in sunflower press bagasse makes the biomass more reactive and independent of heat transfer limitations [23].

2.2.3 Mechanisms of Pyrolysis

During the heating of biomass chemical bonds between polymers are broken and volatiles are released. These are known as the primary reactions. Secondary reactions occur when these volatiles react with each other or undergo additional conversions.

Primary reactions can be split up into three pathways; char formation, depolymerization and fragmentation [24]. Shafizadeh stated that under temperatures of 300^{o}C there was reduction of the molecular weight of compounds by bond scission, removal of water, evolution of carbon monoxide and carbon dioxide, and char [25]. At temperatures higher than 300^{o}C, a tarry pyrolyzate containing levoglucosan in formed including anhydro sugars and oligosaccharides [25,7].

Fragmentation is responsible for the generation of incondensable gas and small chain organic compounds condensable at ambient temperatures. Fragmentation is prominent at temperatures above 300^{o}C and depolymerizes biomass to anhydro-glucose compounds and light noncombustible volatiles [7]. Dehydration is most prominent at lower temperatures (<300^{o}C) and results in molecular weight reduction, water evolution as well as CO, CO_2 and char. Depolymerization is the breakdown of polymers into monomers which result in volatiles that are condensable at ambient temperatures and mostly found in liquid fractions [24]. Charring produces a char which has a polycyclic structure. The main steps involved in the pathway are the formation of benzene rings and the recombination of the rings to form a polycyclic structure [24].

Secondary reactions occur because of instability in the volatiles produced during the primary reactions. These could be attributed to long residence times or low heating rates. Cracking reactions lead to lowering of molecular weights by breaking chemical bonds of volatile compounds. This is a conundrum as the lowering of molecular weight is usually attributed to fragmentation and it is difficult to distinguish which pathway lowers the molecular weights. Secondary recombination reactions can also occur, which is the

complete opposite of cracking; here the molecular weights are increased by recombining volatiles which are no longer volatile in the temperatures of the reactor [24].

2.2.4 Pyrolysis Reactors

1. Fixed bed pyrolysis reactor: These reactors have very low heat transfer and are hence used for the production of charcoal. Their liquid yields are low. They usually operate at long residence times, low gas velocity and high ash removal rates [5]. There are downdraft and updraft fixed bed reactors. In downdraft reactors the biomass particles are inserted at the top of the reactor and meet a flow moving in the downward direction that supports gasification. In the Updraft reactor the downward moving biomass is met by a gas stream moving upwards [4]. They are simple and very reliable. They are typically comprise of firebricks, steel with a fuel feeding unit, ash removal and exit for gas [5] [26]. Their disadvantage lies in their tar removal.
2. Bubbling fluidized bed pyrolyzers: Bubbling fluidized bed reactors are very simple to construct and can achieve good heat transfer to the biomass particles. They produce good quality bio-oil of 60 – 75% weight [7,6], and char accumulation is much less due to it being rapidly eluted. The reason is that char is a vapor cracking catalyst and should be ejected by the use of a cyclone separator. Fluidized bed reactors are comprised of the following: hopper, pyrolysis reactor, cyclone, quench system, electrostatic precipitator and bio-oil tank [7].

3. Circulating fluidized beds and transported bed reactors: These reactors are almost the same as the bubbling fluidized bed pyrolyzers except for the residence time for the products. Because of the high gas velocities the char is removed quickly. However, this can cause the char content to be increased in the bio-oil. The heat transfer rates are not high in these reactors because of gas-solid convective heat transfer. Another type of CFB (circulating fluidized beds) is the twin bed reactor type. Here the second reactor is used to combust char to reheat circulating solids [6]. This causes ash, which is a cracking catalyst for volatiles to be built up in the circulating solids. There are heat transfer limitations with this reactor, thus the particle sizes must be below 3 mm for good liquid yields [14].
4. Rotating Cone reactor: These reactors are mainly used in flash pyrolysis reactions. In this reactor there is mixing of biomass particles with hot sand particles. This mixture is inserted into the base of a cone. Upon the spinning of the cone, centrifugal force causes the larger particles to move upwards towards the lip of the cone and spill over. The products are sent to a condenser and char and sand are combusted and the sand reused in the cycle [5]. Carrier gas requirements are really low except for the combustion of char and sand transport [4] [27]. The liquid yields for dry feed are typically 60-70% [4,19].
5. Auger Reactor: In this reactor augers are used to convey biomass as well as sand into a heated cylindrical tube [4]. The principle of operation is that biomass is continuously pyrolyzed by bringing it in contact with a bulk solid heat transfer medium, aka ‘heat carrier’ [19]. The heat carrier material, which may be sand, is

heated independently before being introduced and mixed in the reactor. The volatiles and products exit at designated ports and the char is transported and stored with the heat carrier [19,28]. Their disadvantage is that they are not feasible on a large scale.

6. Vacuum pyrolysis reactors: These reactors have slow heat transfer rates. They also have very low product residence times like that of fast pyrolysis. Complex organic molecules decompose into fragmented products and are removed by the vacuum. They are then condensed and form pyrolytic oils. The rapid volatilization under vacuum minimizes secondary decomposition reactions [6]. Large particles are required which leads to larger instruments and costs. The liquid yields are 60-65% compared to 75-80% from ablative, fluidized bed, and circulating bed reactors [14].
7. Entrained Flow reactors: These are simple reactors and are based on free fall reactors. The reactors consist of a gas flow which is heated at the top. The sample is inserted and allowed to freely drop. The flow rates are monitored to ensure that particles are isolated from each other [29]. The solid residue is sent to a cup at the bottom and a gas line is used to send the gas mixture to a filter [29].
8. Ablative pyrolysis reactors: This is basically a friction type pyrolysis reactor. It involves the particles hitting and sliding over a hot source. The reaction depends a lot on the heat transfer between the particle and the wall. Therefore, small particle size is required. The pressure applied on the impinging particles causes a shearing action that creates more surface area which allows for better heat

transfer. As the particles are heated and slid over the wall they give out oil which helps in lubricating the next particle in line and it also evaporates rapidly to yield the pyrolysis products. A high pressure of the particles is achieved on the walls because of centrifugal force and the reactor wall temperatures are usually<600^0C [6]. No inert gases are required in this type of reactor therefore processing equipment is smaller. The disadvantage is that the process is surface area controlled, and thus scaling is costly. Also, the reactor is driven mechanically, which is costly [7,14].

9. Plasma pyrolysis reactor: Plasma as the name suggests has a very high working temperature. This sort of pyrolysis favors fast or flash pyrolysis, hence, these reactors are a solution to reducing tarry compounds that are generated in slow pyrolysis. Due to the high temperature a significant amount of heat is lost to the atmosphere by radiation and conduction [4,5]. They are also very expensive compared to other reactors. There are a number of reactors that utilize plasma, they include, plasma entrained fluidized bed reactors, plasma fixed bed and plasma spout-fluid bed reactor [30].
10. Micowave reactor: : These are relatively new and use the energy transfer of a microwave heated bed. The reactors are powered by electricity, which includes the initial drying phase. Inert gas is constantly fed to the system to promote the oxygen free environment. They have good heat transfer and good control of the heating process due to their more uniform temperature distribution which prevents secondary reactions [4,31]. A wide range of biomass types are

acceptable to be processed in microwave reactors and allow high yields of bio-oil and syngas [32].

11. Solar reactor: : These reactors use concentrated solar energy to generate high temperatures (>700^{o}C). They usually consist of a quartz tube with opaque external walls which are exposed to a parabolic solar energy concentrator. There are many concentrators that are used--parabolic dish, Heliostat, Parabolic-trough, compound parabolic, linear Fresnel and Fresnel lens [33]. The main advantage of the reactor is that it does not require fossil fuels or electricity to conduct pyrolysis. Normal pyrolysis techniques utilize the feedstock to generate heat but these maximize the amount of feedstock used [5].

2.3 Bio-oils

Bio oils are dark brown free flowing liquids comprised of a mixture of oxygenated compounds and water from reaction products and from the original feedstock [11,34]. The liquids are formed by rapid depolymerizing of biomass feedstock at very high temperature followed by rapid quenching of the products. The rapid quenching traps many products that would further react if residence times are longer [6]. The liquid obtained is a complex mixture and contains some bit of char as well as guaiacols, catecols, syringols, vanillins, acetic acid, formic acid, and other carboxylic acids [35,6].

Over time bio-oil viscocity increases and a phase separation may occur. This is believed to be due to a breakdown in the microemulsion and chemical reactions that continue to occur in the oil [6]. Bio-oils also contain aldehydes and ketones that can react together to form larger molecules.

Bio-oils have a high heating value of 17 MJ/kg, and although they are referred to as bio-oils, they do not mix with hydrocarbons because of their high polarity and hydrophilic nature [11], [6]. Bio-oils also have a large water content of 25 wt% and a higher oxygen content of 45-50 wt% compared to petroleum oils. Some of the important properties of a typical bio-oil are mentioned in table 1.

Table 1. Bio-oil physical properties [6].

Physical Property	**Typical Value**
Moisture content	25%
pH	2.5
Specific gravity	1.20
Elemental analysis	
C	56%
H	6%
N	0-0.1%
O	38%
HHV as produced	**17Mj/kg**
Viscosity (40^{o}C and 25% water)	**40-100 mpa s**
Solids (char)	**0.1%**
Vacuum distillation residue	**Up to 50%**

2.4 Fourier Transform Infrared Spectroscopy

Fourier Transform infrared spectroscopy is one of the most used analytical techniques for studying substances, be it in the form of liquids, solutions, powders, paste, films, gases and surface, provided a specific sampling technique is used for the analysis [36]. In the *in-situ* study of fast pyrolysis of biomass it is used to give insight on the time evolution of particles as fast pyrolysis occurs.

2.4.1 Interferometer

The interferometer is used to obtain an interference pattern by the superposition of two waves. In the FTIR the basic principle of operation of the interferometer is the splitting up of the beams and making one beam travel a longer distance compared to the other before they combine back and recombine with each other.

The most common interferometer used in FTIR's is the Michelson interferometer. Its working is given below in the figure.

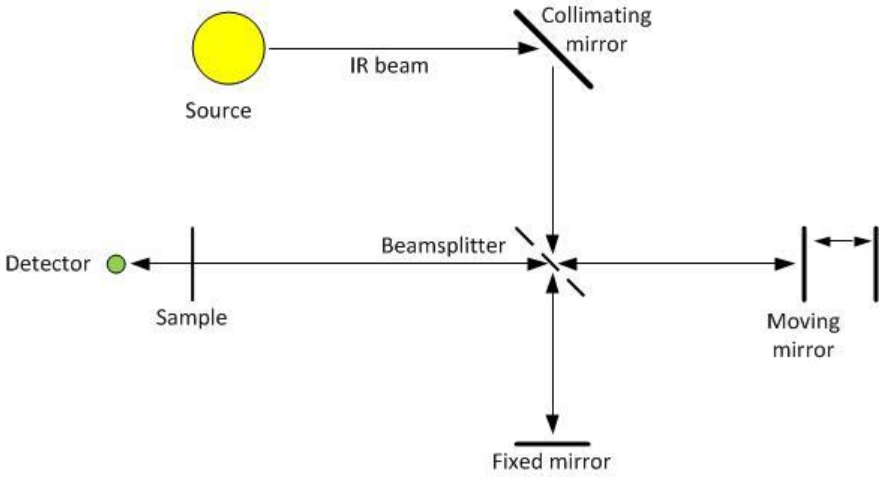

Figure 2. Schematic of Michelsons interferometer.

The interferometer consists of 4 arms. The top arm consists of the source and the collimating mirror. The collimating mirror is used to make the beams parallel. The bottom arm consists of a fixed mirror that does not move. The left arm consists of the sample and the detector. In the middle is the device used to create two beams, called the beam splitter. The beam splitter splits the beam and sends one beam to the fixed mirror and the other to the moving mirror on the right arm. The beam which passes through the sample and to the detector is the transmitted beam and the beam which is reflected away by the splitter is the reflected beam. Beam splitters are usually made of KBr or Cs_2O and coated with germanium or iron oxide [37,36]. An ideal beam splitter is one that allows 50% of the beam to pass through it and reflects back 50%. The beam splitter material is chosen according to the region being examined. Germanium and iron oxide are coated on infrared transparent substances such as potassium bromide to produce beam splitters for mid- and near-infrared regions [36]. The moving mirror produces optical path differences periodically between the two arms and results in the formation of interference patterns. There are two types of interference patterns.

1. Constructive interference: Here the recombining beams have amplitude greater than either of the individual split beams. The light beam reflected from the fixed and the beam reflected by the moving mirror has zero path difference. In this case the beams will recombine at the beam splitter and the crests will overlap. The two light beams are said to be in 'n' phase with each other and have amplitude equal to the sum of the amplitudes of the reflected beams.

$$\delta = n\lambda \qquad (1)$$

Where $\delta = Optical\ path\ length$

n = any integer

as long as the two beams have whole number values of 'n', then constructive interference will occur [38].

2. Destructive interference**:** When two beams are out of phase with each other and recombine, their respective amplitudes cancel each other out. This results in a beam with amplitude lower than either of the reflected beams. Equation 7 gives the optical path difference of destructive interference if n is any integer from 0 to infinity [38].

$$\delta = \left(n + \frac{1}{2}\right)\lambda \qquad (2)$$

2.4.2 Infrared Spectrum

Infrared radiation is an electromagnetic wave. When a certain wavelength of the radiation is incident on a molecule, the only way the molecule can exhibit any infrared activity, such as the absorption of radiation, is if there is a net dipole moment in the molecule or functional group under study [39] [38]. A dipole is dependent on the vibrations of the molecule. A molecule has a number of vibrations such as symmetric and asymmetric stretching. Bending includes deformation, rocking, wagging, twisting, out-of-plane bending and in-plane bending. In general depending on if the molecule is linear or nonlinear, it will have a total of 3N degrees of freedom which is the summation of the vibrational, translational and rotational modes and where N is the total number of

atoms [38] [39]. This is not always true with most atoms because there can be redundant modes of vibration, or the energy absorbed may be the same. So in most spectra when we see a sharp peak at a certain wavenumber it means that at that wavenumber some bond has absorbed the incident infrared radiation at that wavelength. The higher the peak the more is the absorbance.

2.4.3 Transformation of the Interferogram to Spectrum

The transformation of the interferogram to a spectrum happens by using Fourier transformations. Fourier's theorem states that many mathematical functions can be expressed as a superposition of sine and cosine waves [6].

The equations that relate intensity and spectral power density are

$$I(\delta) = \int_0^\infty B(\vartheta)\cos(2\pi\vartheta\delta)\,d\vartheta \qquad (3)$$

$$B(\vartheta) = \int_{-\infty}^{\infty} I(\delta)\cos(2\pi\vartheta\delta)\,d\delta \qquad (4)$$

Where ϑ is a particular wave number. Equations 3 and 4 are taken from Refs. [37] [36] [40] [41].

The above two equations are known as the Fourier pair and they are interchangeable. Equation (3) gives the relation between intensity as a function of path length difference and Equation (4) gives the relation for the variation in intensity as a function of wave number [7]. Fourier transforms when applied to a function invert the x-axis of the function. Therefore, when an interferogram is Fourier transformed it transforms a plot of intensity vs. path difference to a plot of intensity vs. wavenumber (cm^{-1}).

The basic procedure now is to create an interferogram without a sample and then with a sample. The reason for the initial interferogram is to do a background of the atmosphere. The latter is for the material of study. If the background is the same during the scan for the material then the 'other' materials will not show.

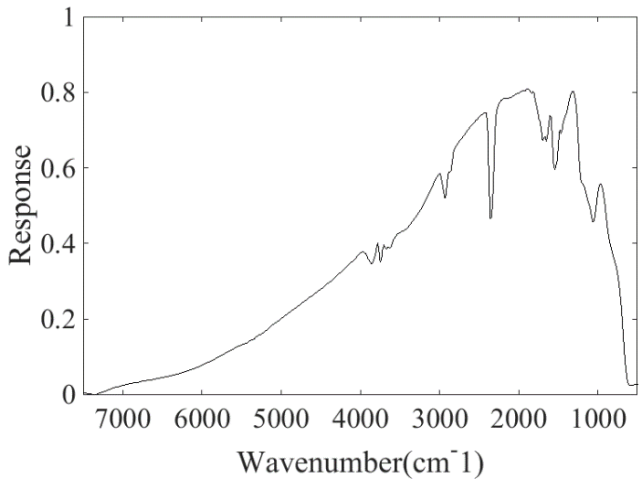

Figure 3. Typical background spectrum with nitrogen purge.

The interferogram is produced by moving the mirrors. It is an analog signal at the detector. The next phase is digitizing the signal. Here there are two errors that can occur. First, the transformation requires the integration over a finite displacement rather than an infinite displacement [36]. Another source of error is if the sample intervals are not exactly the same on each side of the maxima corresponding to zero path difference [36]. Here phase correction is the method of ensuring that sample intervals are the same on each side of the maxima.

The resolution of a FTIR spectrum is proportional to the maximum path difference between two beams. The limiting resolution is the reciprocal of the path length

difference. One would think that it is easy then to get good resolution but it is not the case because precision in optics becomes harder at longer displacements and path lengths [7].

One of the main problems to address in using FTIR is increasing the signal-to-noise ratio (SNR). One of the most widely used methods to increase SNR is the signal averaging method. There are a lot of parameters that can be optimized to give good SNR. Their relationships are seen in the following equations:

$$SNR \propto N^{\frac{1}{2}} \quad (5)$$

$$SNR \propto Res \quad (6)$$

$$T \propto N \quad (7)$$

$$T \propto \frac{1}{Res} \quad (8)$$

where N is the number of scans, *Res* is resolution of scans and *T* is the total time of scanning. Equations (5,6,7, and 8) taken from [36] [38].

2.4.4 Beer-Lambert Law

This law states that the amount of light transmitted by a sample is based on the thickness of the sample. With respect to solutions or gases it states that the absorbance is directly proportional to thickness and concentration of the sample [38] [36].

$$A = \in cl \quad (9)$$

Where A is absorbance of the material, c is the concentration and *l* is the thickness or path length of the sample, and ∈ is the constant of proportionality called molar absorptivity. This molar absorptivity is an intrinsic quality. Knowing the path length absorbance and absorptivity one can calculate the concentration of a species in the sample.

2.4.5 Spectral Interpretation

In the analysis of the spectral data obtained, one must understand the origins of the data and how it came about. Firstly, every molecule vibrates. The degree to which it vibrates determines the dipole that it is capable of achieving. Only when a particle under study has a net dipole moment will it be able to absorb energy and thus give the absorption spectra that we see. In general there are various vibrations in a molecule such as, symmetric and asymmetric stretching and bending which includes deformation, rocking, wagging, twisting, out-of plane bending, and in-plane bending. [36]. The number of normal modes of vibration are 3N-5 for linear and 3N-6 for non-linear, where N is the number of atoms [36] [39]. Now, in reality if we applied this formula to a nonlinear molecule, since they are most abundant, and if we obtained the modes of vibration, the actual number of absorptions would not be the same. This is due to the fact that there would be many symmetric and asymmetric vibrations but the vibrations would be redundant because the same amount of energy would be needed. Also symmetric molecules have fewer infrared-active vibrations because of the fact that they will not be able to generate strong dipoles [36].

The first step in spectral interpretation is looking at the overall spectrum and assessing the number of peaks. If the number of peaks is less, than the compound could be a low molecular weight organic or inorganic compound [39]. If the bands are broad then that could be due to hydrogen bonding such as water solutions, alcohols, etc. The next step involves the checking of the 3200-2700 cm^{-1} region. Characteristic peaks in this region are due to carbon and hydrogen containing species. Species above 3000 cm^{-1} are usually aromatic compounds and below 3000 are aliphatic [9]. The next band is between 3650-3250 cm^{-1}; if there are sharp peaks in this region that usually suggests the occurrence of an alcohol or phenol [39]. Testing for carbonyls is done in the 1850-1650 cm^{-1} range which is the next step in spectral analysis; in the lower regions of 1650 cm^{-1} there could be the detection of ring structured compounds [39] [9] [42]. The next step is the testing of aromatics. These give distinct peaks in the 1615-1495 cm^{-1} region.

The testing for species in FTIR is very difficult with respect to complex mixtures of compounds. Many compounds share similar bonds and hence absorb at those wavenumbers. Methods such as GC-MS and GC-FID should be integrated in the process to determine the actual compounds being formed. Below is a table of the common absorptions that are important in the study of biomass pyrolysis FTIR.

Table 2. Typical functional groups and associated wavebands.

Wavenumber (cm^{-1})	**Functional Groups**	**Compounds**
3600-3000	OH stretching	Acid
2860-2970	C-H stretching	Aliphatic
1700-1730	C-H stretching	Aromatic
1632	C=C	Benzene stretching
1440-1400	OH bending	Acid
1215	C-O Stretching	Phenol
700-900	C-H	Aromatic hydrogen

2.4.6 Advantages of FTIR

1. One of the major advantages FTIRs enjoy over other infrared spectrometers is their ability to measure spectra with high signal-to-noise ratios.
2. A second advantage FTIRs enjoy compared to other infrared spectrometers is the *multiplex advantage*. The multiplex advantage basically calls the FTIR spectrometer as an array of multiple monochromators designed to detect a specific wavelength. All the monochromatic detectors are identical except for the orientation of each grating that gives different wavelengths. This is an advantage because the time taken by an FTIR is much less compared to a dispersive spectrometer.

3. Conne's advantage: There will be errors caused by moving mirrors displacement on the interferometer. This can be resolved with an FTIR using monochromatic interferometry [41].
4. In an FTIR the stray light does not cause spectral intensities. However, artifacts can be produced and must be avoided.

2.4.7 Disadvantages of FTIR

1. 'Artifacts' are the disadvantages seen in an FTIR. They are features present in the sample that are not of the sample. For example, water vapor and carbon dioxide are often present outside the sample region and can lead to spurious signals. The only way to rule these out is to run a background scan. If the concentration of the artifacts remains the same after the background scan then they will ratio out. However, background scans and sample spectra must be taken at different times. If the concentrations of water vapor and carbon dioxide change, then it will lead to contamination of the spectra [38].

2.4.8 Pyrolysis FTIR Studies

There have been a large number of studies conducted on the pyrolysis of biomass. These studies have been coupled with various diagnostic tools. The most common tools used have been Thermo-Gravimetric Fourier Transform Infrared Spectroscopy (TG-FTIR) and Gas Chromatography Mass Spectrometry (GC MS). Very few researchers have studied the *in-situ* evolution of pyrolysis products. Li, et al. was able to couple a reactor with a rapid scanning FTIR spectrometer and study the product evolution of filter

paper [43]. His reactor had two heating zones to study, including the primary as well as secondary reactions. The reactor had a variable flow rate to vary residence times in the reactor. Siencgchum et al. was able to study the *in situ* pyrolysis of coconut biomass using a Diffuse Reflectance Fourier Transform (DRIFT) cell [44]. The DRIFT cell is placed inside the FTIR housing itself and had a heating rate of 83^{o}C and was heated from room temperature to 580^{o}C.

Most of the FTIR tests other than those stated above have been done using the TG-FTIR. Xiaoxiang, et al. studied the pyrolysis of low molecular mass (LMM) and high molecular mass (HMM) lignin using TG-FTIR and were able to obtain spectra of the pyrolysis products as well as study the activation energies of different lignin samples [42]. Haiping, et al. used a packed bed pyrolysis reactor coupled with TG-FTIR to study the pyrolysis of cellulose, hemicellulose, and lignin and their respective gas evolutions [9]. Qian et al. used TG-FTIR to study Van Soest analysis of strong acid detergent fiber of wood lignin and studied the evolution of products at two stages--a lower temperature with activation energy of 70-90 kJ/mol and higher temperature with activation energy of 135-142 kJ/mol [45]. Hui Zhou, et al. conducted TG-FTIR pyrolysis studies on municipal solid wastes such as rice, poplar wood, and PVC and recorded the interactions of each of the wastes with each other [46]. Supeng, et al. used TG-FTIR to study the pyrolysis of cyanobacteria and used the Popescu method to determine the best kinetic model for the pyrolysis [47]. Fu, et al. developed a reactor made of quartz heated by a carborundum heater and coupled with a gas analyzer and FTIR to study the pyrolysis of Maize stalk, rice straw, and cotton straw at temperatures of 900^{o}C at a rate of 10^{o}C/min

[48]. Lee, et al. used FTIR to study the kinetics of pyrolysis of swithgrass as well as the product evolution [49].

All the above studies utilized the FTIR for both evolution studies as well as kinetic studies. However, only Li, et al. was able to rapidly heat the sample by sudden introduction into a high temperature region.

CHAPTER 3. EXPERIMENTAL SETUP

3.1 Pyrolysis Reactor

In the figure below is the exploded view of the bench scale pyrolysis reactor that was designed and fabricated for *in-situ* testing. The abilities of the instrument include:-

1. Optical access for laser diagnostics.
2. Ability to reach and maintain 500^{o}C temperature.

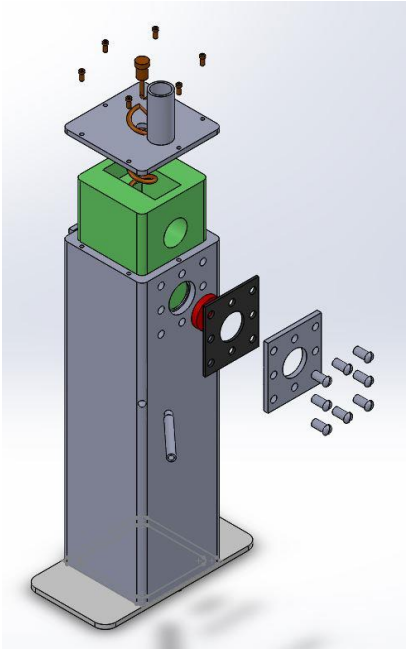

Figure 4. Exploded view of pyrolysis reactor.

3. Sample insertion that allows for the biomass to heat rapidly in the surrounding pyrolysis atmosphere.
4. Variable flow speeds to control product residence times.

Figure 5. Pyrolysis reactor.

The exterior of the reactor is constructed from 304 stainless steel square tubing of side 76.2 mm. The interior dimensions of the tubing are 63.5 mm giving it a thickness of 6.34 mm, the height of the reactor is 254 mm. As can be seen from Figure 4 two recessed holes of 25.4 mm diameter are drilled on to two faces of the steel. This is used to hold the Kbr windows that are used to transmit mid-IR radiation. In Figure 4 the red disc is the window. On top of the window is a high temperature resistant silicone gasket attached by the help of 8 tapped holes on both faces. This is done to prevent gases from escaping the reactor, and finally a 304 stainless steel block with a through hole of 0.9” is cut out and held on top of the gasket with the help of 8 tapped screws. The interior of the reactor is made of 4 ceramic blocks that come together to form a long cuboid. The

ceramic utilized is glass-mica ceramic from McMaster-Carr and is used to obtain isothermal conditions within the reactor. In the center of the cuboid is a cavity that runs through the whole length of the cuboid of 20x20 mm dimensions. This cavity will continually be referred to as the pyrolysis cavity. This cavity houses a heating coil to heat the biomass as seen in the figure. The cuboid also has a 1" through hole that aligns with the holes on the exterior. The heating coil is pitched in such a way that the coils do not interfere with the acquisition of data. The top of the reactor is held in place by 8 tapped screws, and the top is also made of 304 stainless steel and has an exhaust setup for the removal pyrolysis gases. Lastly, a sample insertion tube is seen at the corner of the instrument, it is pipe threaded to maintain air tightness and can be removed during the cleaning of the instrument.

The heating of the biomass is done primarily by a coil heater. An Entherm 690 Watt 965 mm resistance wire of cross section 2.2 x 4.2 mm was bent to the desired coil requirements. The ability of the pitch to be changed on a coil heater was important in the design of the reactor as it does not obstruct the IR beam passing through the reactor. The coil heater was powered by a 120-230V step up transformer from Simran. This was controlled by a temperature controller. Two K-type thermocouples from Omega Engineering are used to determine the temperatures in the reactor, and one of the thermocouples is placed near the sample insertion. This thermocouple is 75 mm from the center of the window. This thermocouple is connected to the temperature controller, which in turn regulates the temperature by switching the coil heater on and off. The other thermocouple is placed below the optical access window and approximately 38

mm from the center of the window. Through the bottom of the reactor hot nitrogen gas at 450-490^{o}C is passed in order to carry away the pyrolysis products. This Nitrogen gas is heated by a self-constructed heater made of heat tape from McMaster-Carr with power of 312 W over a 3/8th in. outer diameter copper tube. This setup allows for a heating rate of 330^{o}C/s into the sample at both product residence times. The setup was covered by a high temperature fiberglass insulation to prevent heat loss. This is heater was made due to the fact that commercial heaters could not provide the temperatures required at very low flow rates.

3.2 Sample Holder

In the design of the sample insertion device it was critical that the device be able to hold the sample in the reactor in a 500^{o}C atmosphere and not conduct too much heat away from the reactor. To do this, a ceramic called zirconia was used. It was chosen because of its low thermal conductivity and high strength. Within the zirconia tube is another ceramic rod made of alumina. This holds two steel wires of diameter 0.8mm. The distance maintained between the two wires is 2 mm. A steel foil from McMaster-Carr is cut to size and bent to a 'V' shape. This steel foil has a thickness of 0.0254 mm. It was important to use such a thin sample holder to improve the heat transfer through it. It should be noted that the heat transfer rate into the sample holder was approximately 330^{o}C/s. The steel foil is then placed between the two wires and held in place by the frictional force of the steel on the wire.

During a test run the steel foil is bent and placed in an aluminum block with a slot of 4 mm width and 3 mm depth cut out. This is weighed using an Acculab L-series scale and then zeroed. The biomass is then added up to the required weight and then placed in the sample holder. Below in Figure 6 is a picture of the sample holder and the sample insertion.

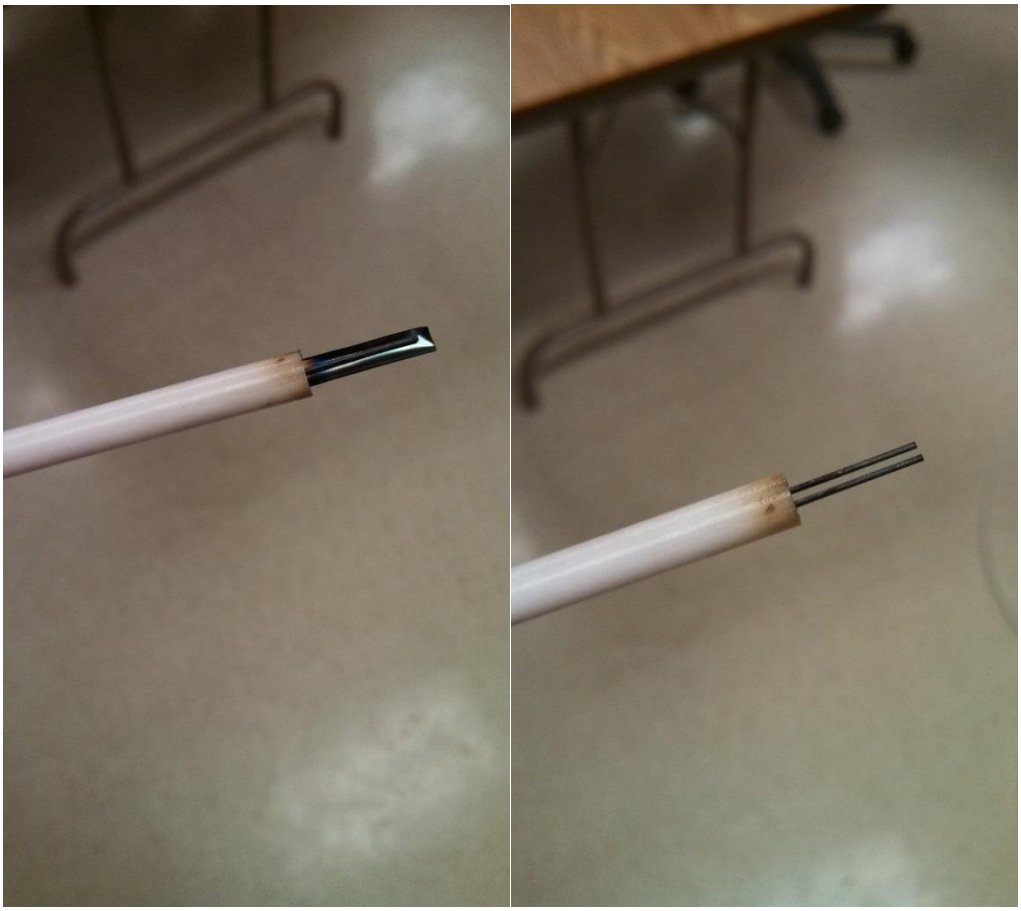

Figure 6. Sample holder on right attached to sample insertion device.

3.3 Experimental Configuration

Given the height of the pyrolysis reactor, it could not be placed in the sample compartment of the FTIR. Therefore, the beam would need to be pulled out of the

spectrometer and passed through the pyrolysis reactor. Figure 7 below is top view of the configuration used.

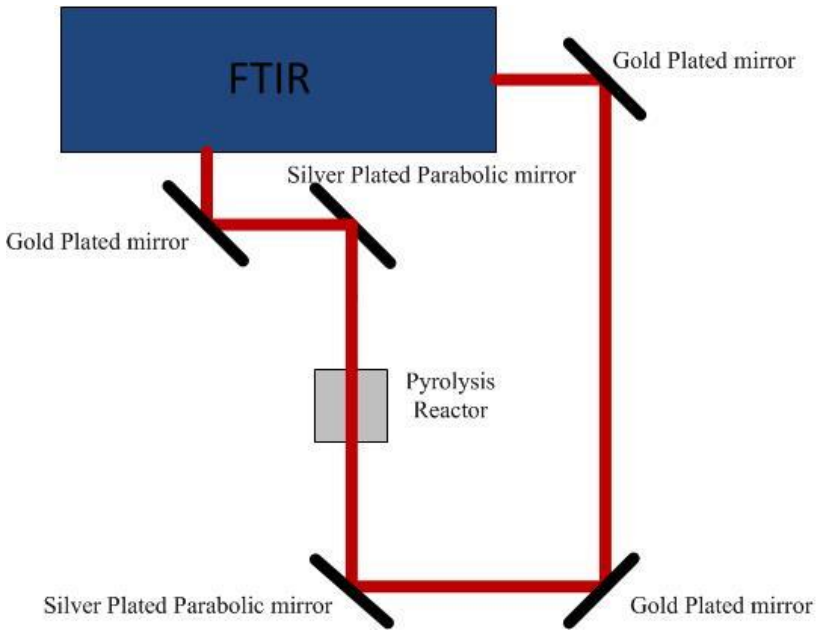

Figure 7. Top view of FTIR setup.

To direct the beam outside of the Varian 680 FTIR, a plane mirror was installed internally that would pop up when the configuration was selected. The beam path was protected by a 4 inch diameter PVC piping and simple air tight boxes were used as enclosures for IR reflective gold plated mirrors. These mirrors were used to direct the beam to the detector. Alongside the reactor were two silver plated parabolic mirrors with focal length 6 inches, which were used to focus the beam into the reactor at a fixed height above the reaction zone and collimate the beam as it exited the reactor. The beam height and sweep gas flow rate determined the residence tie of the products at the time of measurement. The beam size was determined experimentally to be 0.1 inches while entering the reactor. Two zinc selenide windows purchased from THOR labs were used

as the optical access points of the cell. Zinc selenide had good temperature resistance as well as good transmittance for mid-IR. The reactor was placed in an enclosure made of plexiglas and a nitrogen purge was introduced into the setup at three different points--one at the point where the beam was directed out of the cell, one into the plexiglas enclosure, and one into a box that held a mirror that directed the beam into the FTIR. Within the FTIR, the detector was changed from a DTS to a MCT (mercury telluride) detector which allows for higher frequency data acquisition. This detector is required to be liquid nitrogen cooled as it heats up very quickly. Based on the data provided by Varian, a resolution of 16 cm^{-1} was used as well as sampling speed of 75 kHz. This allowed for spectra to be obtained in intervals of 0.06 s**.**

CHAPTER 4. RESULTS AND DISCUSSION

4.1 Temperature Profile

To characterize the reactor, the internal temperatures were recorded for 10 minutes and plotted at three different flow rates. The flow rates were changed in order to obtain varying product residence times. The temperatures were measured at two distinct locations. One being 38 mm from the center of the window and the other being 75 mm from the center of the window as well as being 20mm below the sample insertion. In the initial tests the two residence times chosen were, 0.9 s and 1.45 s. These corresponded to Figures 9 and 10 below. In the second phase of tests in which the internal structure of the reactor was changed, the heat profiles corresponded to Figures 8 and 9 for residence times 0.9 s and 1.45 s approximately**.**

The temperature profiles are formed due to internal coil heating as well as the heated flow of nitrogen from the bottom of the reactor. From Figure 8 it can be seen that the temperature differences between the two thermocouples reach a maximum of 35^{o}C. From Figure 9 it can be seen that the temperature difference reaches 32^{o}C and from Figure 10 the temperature difference obtained is 21^{o}C. As we can see as the flow rate is increased the difference in temperatures is decreased.

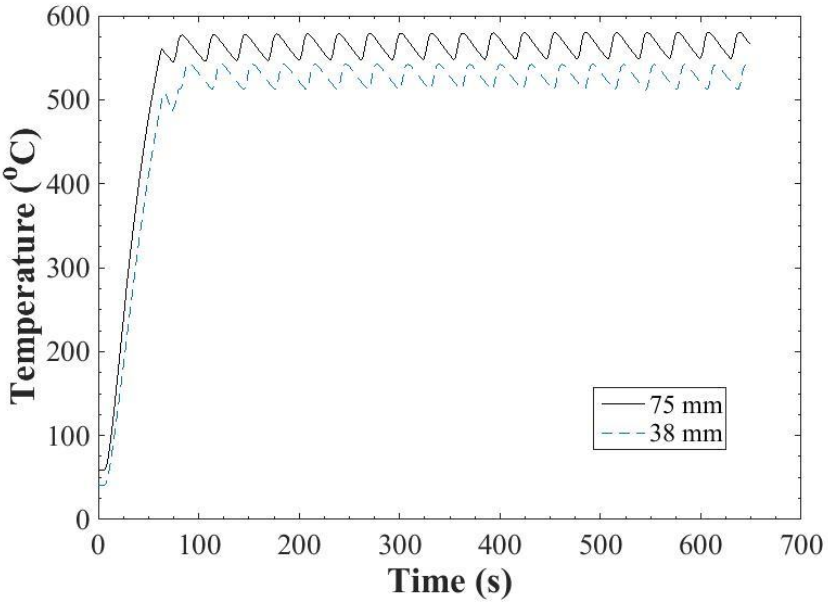

Figure 8. Temperature profile inside modified pyrolysis reactor with product residence time 1.45 s.

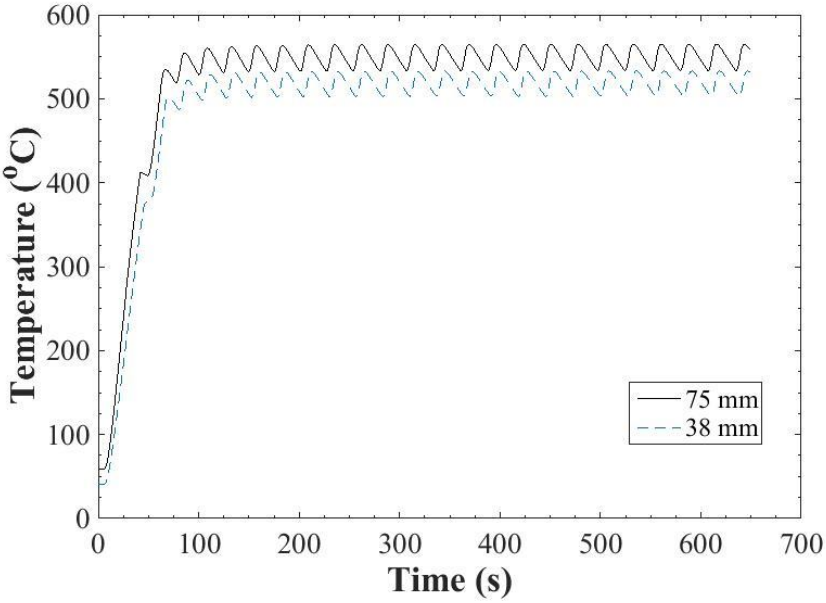

Figure 9. Temperature profile inside reactor at 1.45 s product residence time and 0.9 s product residence time for modified reactor.

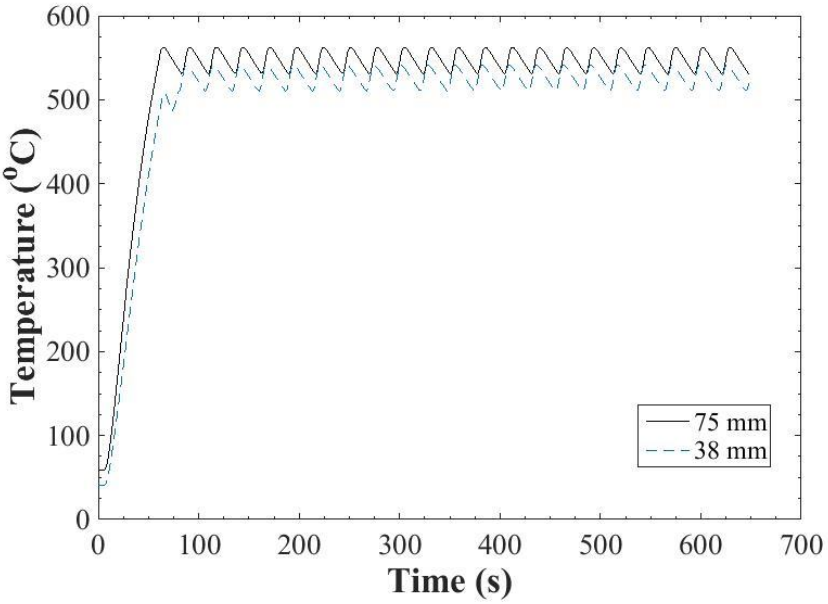

Figure 10. Temperature profile inside reactor at 0.9 s vapor residence time.

4.2 FTIR Tests

In the initial tests 5 mg of cellulose from Sigma Aldrich was used as the standard feed in the cellulose experiments. The setup was started and allowed to reach isothermal conditions inside the reactor. The sample would then be placed in the holder and the data acquisition in the FTIR would be started. The sample would then be inserted into the reactor and left in the reactor for the duration of the experiment, which would usually be 45–60 s. Longer times were not used because the data acquisition system would become unstable and the software would sometimes switch off.

4.2.1 Cellulose Tests

Cellulose tests were done at two residence times and the data obtained is seen below. In figure 11 the cellulose spectra were extracted at points in which the evolution of CO_2 was maximum. This was done using the Agilent software package and picking the plots based on the evolution vs time plot. The extracted spectra were then weight averaged using the Matlab function and plotted.

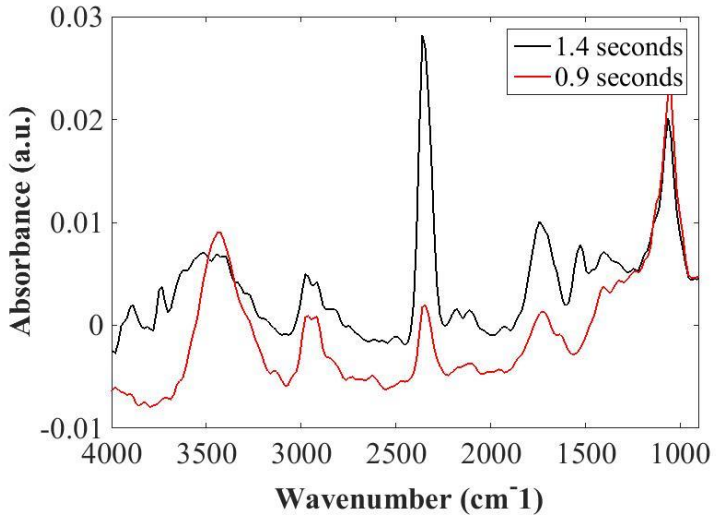

Figure 11. Cellulose pyrolysis spectra at 0.9 and 1.4 s residence times.

The first highest peak that is seen above is the CO_2 peak at 2363 cm^{-1}. The absorbance of this peak is higher at longer product residence times. CO_2 is proposed to be produced by the cracking of C=O bonds [44]. The small peak seen to the side of CO_2 is CO at wavenumber 2167cm^{-1}. Its release is due to the cracking of carbonyl (C-O-C) and carboxyl (C=O). The CO peaks are also seen to have higher absorbance at longer product residence times. The next major peak is that of CH_4 and occurs at 3017 cm^{-1} and can be caused by cracking of methoxyl groups -O-CH_3 [9]--this is the region of C-H

stretching. According to Coates, the peaks at the range of 1750-1700cm^{-1} show the presence of a simple carbonyl compound such as a carboxylic acid or aldehyde [39]. The only peaks that show higher absorbance at shorter product residence times are 1500 – 900 cm^{-1} and 3500-3200 cm^{-1}. They are due to skeletal vibrations of C-O and show the existence of what could be esters and formic acid and O-H stretching, respectively [10] [50]. Taking under consideration the Beer-Lambert law, the sample sizes were kept the same and the path lengths did not change; therefore the above plots could give insight to the concentrations of certain species at different residence times.

4.2.2 Lignin Tests

The tests with lignin were carried out the same way as that of cellulose. 5 mg of sample was weighed and pyrolyzed. Figure 12 is the FTIR spectra of lignin taken at residence times 0.9 sand 1.4 s.

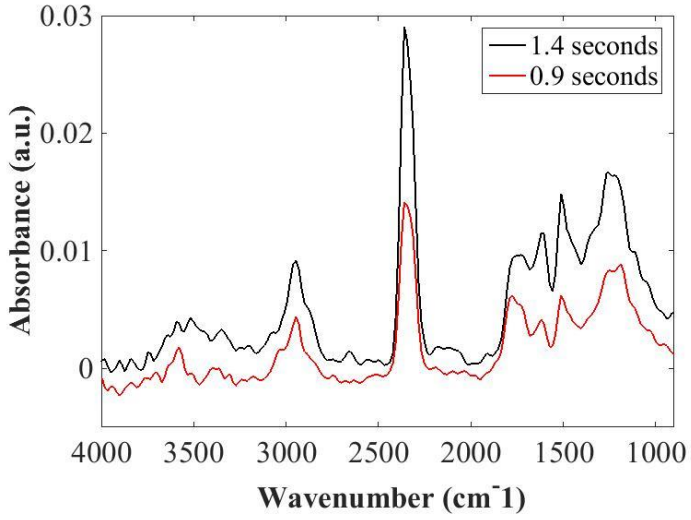

Figure 12. Lignin pyrolysis spectra at 0.9 and 1.4 s residence time.

From the above figure we can see the highest peak of CO_2 occurring at the 2217-2391cm^{-1} range. The release of CO_2 can be attributed to the breaking of the lateral lignin chains. The bands 2850-3200 cm^{-1} show the generation of methane. Methane can be generated by the breaking of methoxyl bonds, break of -CH_2- or the secondary pyrolysis of volatiles [42]. But, since the reactions are in the fast pyrolysis range the method can be overlooked. Previous studies show that bands 1300-1400 cm^{-1} show the release of volatiles, however the region 1300-1800cm^{-1} is also the range for water release, the previous studies used TGFTIR so the heating was slowly ramped up over time therefore, the dehydration stages could be noticed [42] [45]. Another problem faced is that if volatiles are being released, the structure of lignin is very complex and many functional groups will be contained in the phenols such as gauiacol, methoxyl and alkyl groups [45]. The CO band is seen at 2112- 2180cm^{-1}. The absorbance of CO is seen to increase at higher residence times. Unlike cellulose all the peaks of lignin at the shorter residence times stay below the peaks of lignin at longer residence times.

4.3 Evolution Tests

4.3.1 Cellulose Tests

In these tests the evolution of products were analyzed during pyrolysis. The Varian 680 FTIR software has the ability to plot the intensity of designated regions of spectra with respect to time. These plots help understand the initial staring point of the evolution of the bond groups under study. The chosen peaks under study were centered at 2150, 2320, 2940 3430 and 1720 cm^{-1} and pertained to CO, CO_2,CH, C-O and carbonyl bands respectively. The sample sizes that were used were 1, 2, 4 and 8 mg, and again were

conducted at two residence times. Figures 13 to 17 show the evolution of cellulose pyrolysis products at specified regions and at residence times equal to 1.4 seconds. Later, characteristic rise times are compared for the different spectral regions to infer the relative reaction time of various products. It should be noted that each mass loading test was done separately and in unequal insertion times.

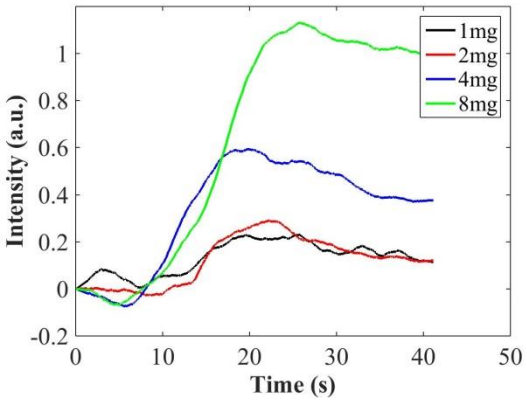

Figure 13. Evolution plots centered around 1720 cm^{-1}.

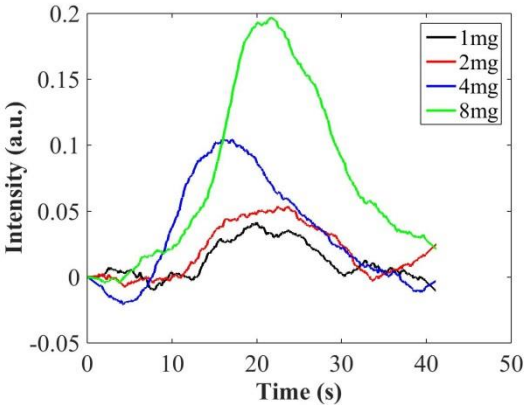

Figure 14. Evolution plots of CO

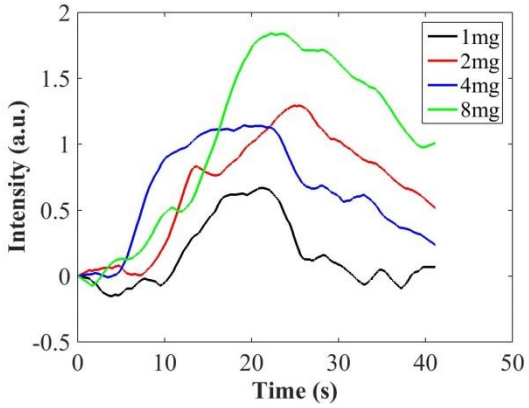

Figure 15. Evolution plots of CO_2.

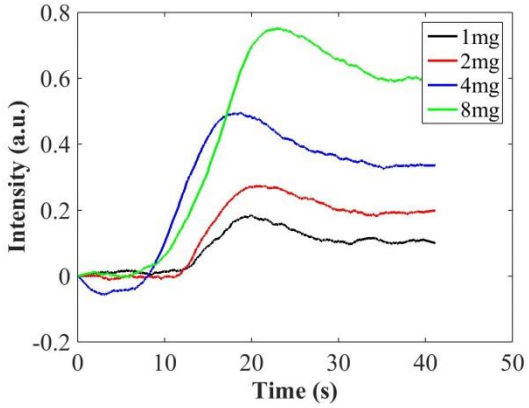

Figure 16. Evolution plots centered around 2940 cm^{-1}.

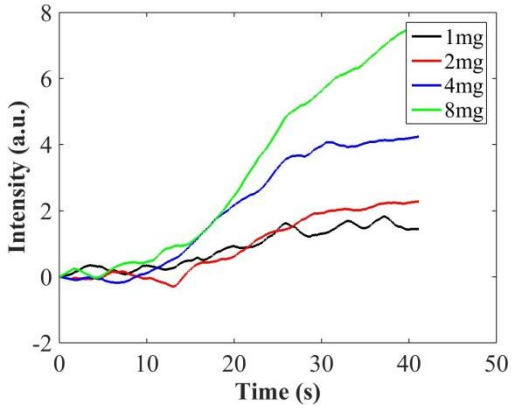

Figure 17. Evolution plots centered around 3430 cm^{-1}.

4.3.2 Lignin Tests

Sample weights of 1, 2, 4 and 8 mg were used in the studies and pyrolyzed in the reactor. The bands that were studied in these tests were centered at 2150, 2320 and 2940 cm^{-1}. They correspond to absorptions of CO_2, CO and CH bands. The tests were conducted at two residence times. Figures 18 to 21 show the evolution of these bands at residence time 1.4 seconds.

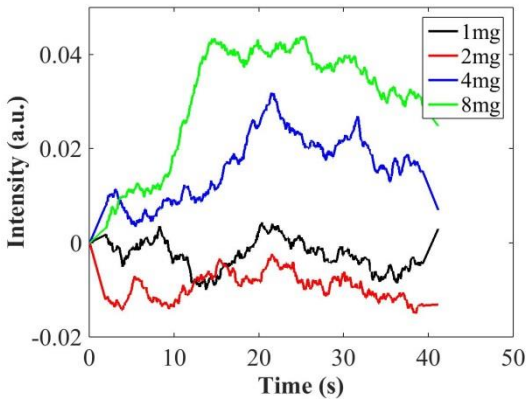

Figure 18. Evolution plots of CO.

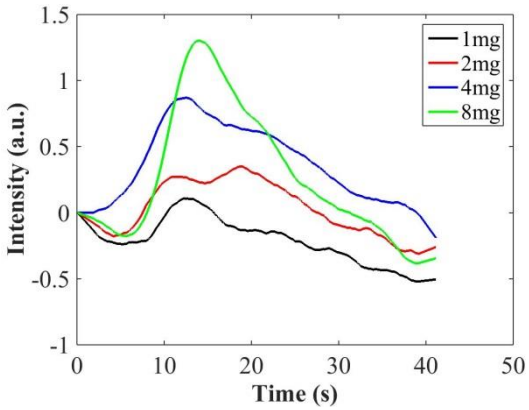

Figure 19. Evolution plots of CO_2.

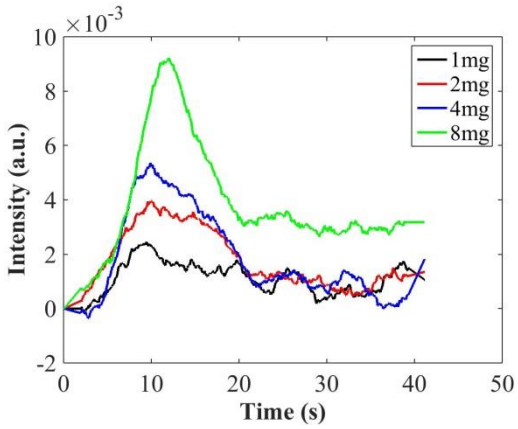

Figure 20. Evolution plots centered around 1747 cm^{-1}.

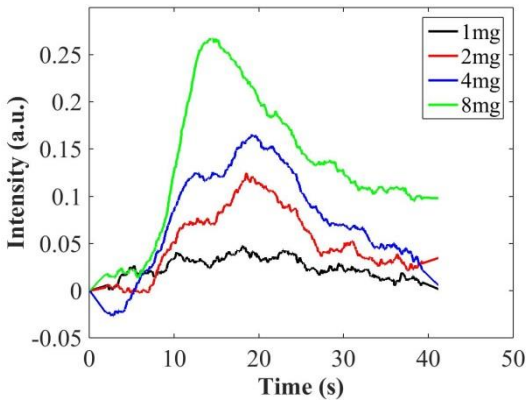

Figure 21. Evolution plots centered around 2940 cm^{-1}.

First, it is evident that the different spectral regions are indeed evolving over time during the reaction, indicating that the spectra are tracking the time dynamics of product formation. Furthermore, there appears to be a peak in the product concentrations. However, as seen in Figures 13–21, some of the intensities of products go to a negative before going to a positive. This can be attributed to the phenomenon of recirculation of products inside the reactor. To truly quantfy the times at which different regions of spectra evolve it is important to have no recirculation. Another problem that can be seen

from the plots is that many of the intensities do not show a tendency to decrease with time. This was seen mainly in the pyrolysis of cellulose. In the pyrolysis of cellulose there was noticeable fogging up of windows as the tests progressed and the spectrum of the fogged up windows is shown in Figure 22. The spectrum shows peaks at the wavenumbers of 3430, 1720 and 1100 cm^{-1} these spectra greatly resemble that off cellulose or levoglucosan meaning that some particles of cellulose are unpyrolyzed and carried away by the sweep gas or that it is a tarry pyrolyzate of anhydro compounds such as levoglucosan. Based on the flow rates the buoyant forces acting on a cellulose particle are more than that of the forces of gravity.

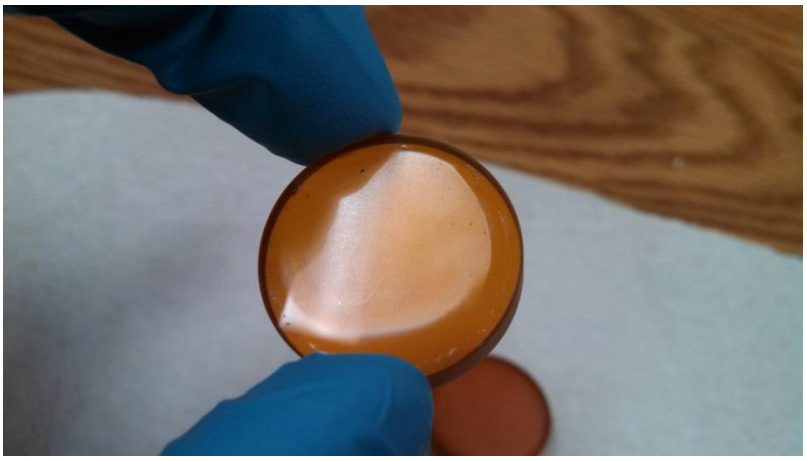

Figure 22. Photograph of window with condensate.

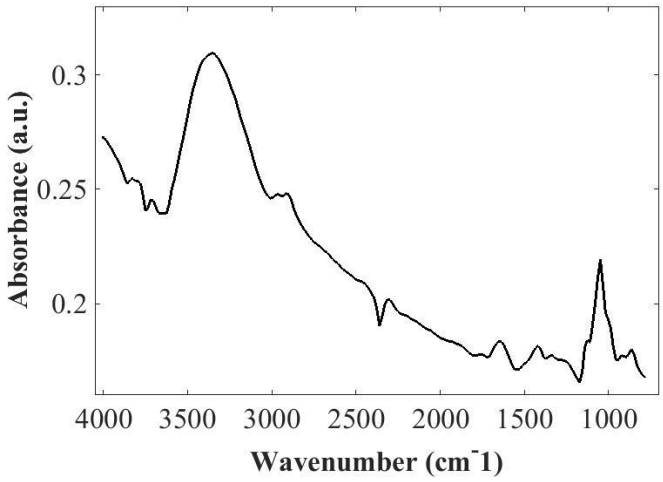

Figure 23. FTIR spectrum of window after operation of the reactor.

4.3.3 Recirculation Test

To test for recirculation, acetylene gas was let into the reactor at a short burst following nitrogen gas. The acetylene evolution was studied over a large period of time and showed a tendency to decrease but not reach fully to zero. Then the reactor was allowed to purge for a minute and another background was taken followed by an evolution test without imputing acetylene. Figure 24 shows the evolution plots for acetylene (left) and after the system was allowed to purge (right) for some time. As we can see from Figure 24, the intensity of acetylene starts at zero and decreases thus showing that at such low flow rates the recirculation is significant.

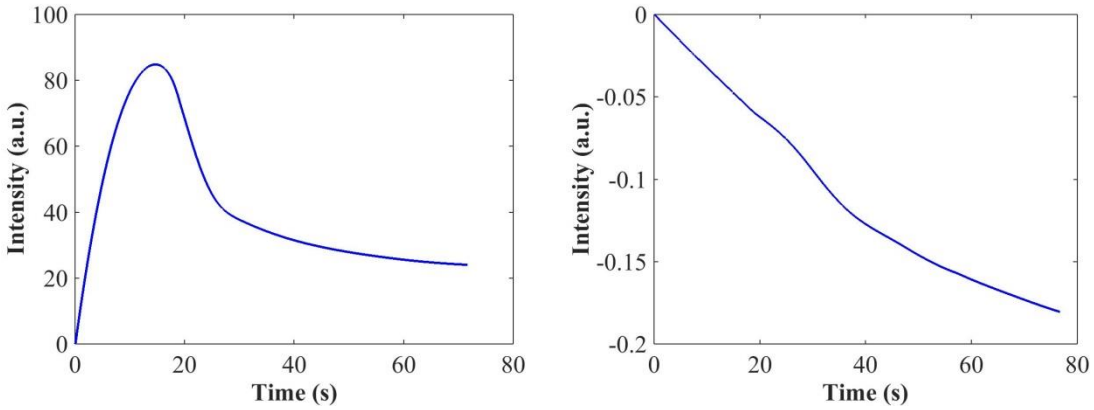

Figure 24. Acetylene gas evolution measured using the FTIR instrument.

4.3.4 Pyrolysis Reactor Modifications

To curb the problem of recirculation, the windows that allow for optical access into the reactor were pushed into the reactor by half an inch each, which reduced the path length by an inch and the resulting plots were obtained. The windows could not be pushed in further because the ceramic used had hardened on the surface surrounding the pyrolysis cavity, and only a diamond tooling would be able to machine the ceramic at that point. Given the time constraints and the tooling at hand, the windows were moved inside by only 0.5 inches on each side. Figure 25 shows the changes made to the ceramic insulation inside of the reactor. The outer skeleton of the reactor was kept intact except for the optical access hole which was enlarged from 0.9 in to 1 in. To keep the windows air tight and prevent products from escaping through that region, two macor ceramic rods were drilled through and placed between the windows and the outer walls of the reactor.

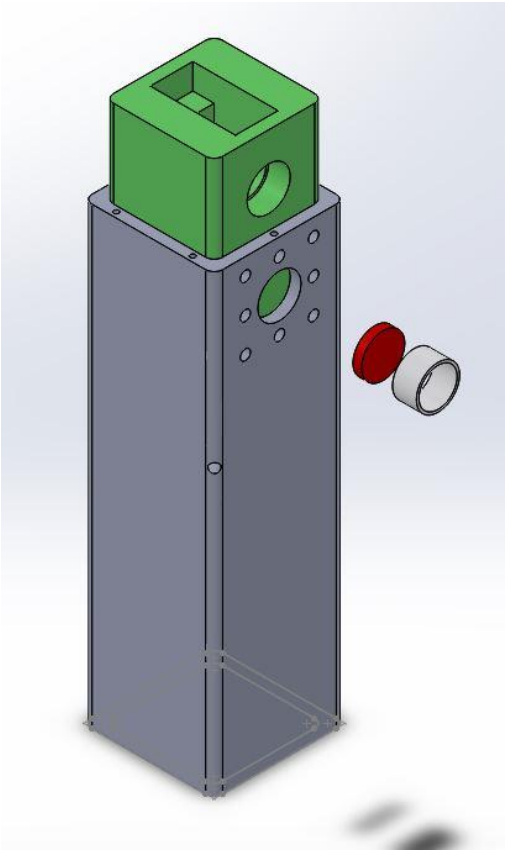

Figure 25. Exploded view of reactor showing new window placement.

4.4 New Reactor FTIR Tests

4.4.1 Cellulose Tests

Figure 26 gives the spectral profile of 4 mg of cellulose pyrolyzed at residence times of 0.9 and 1.4 seconds. Again the spectra were collected at points where the CO_2 evolution was highest.

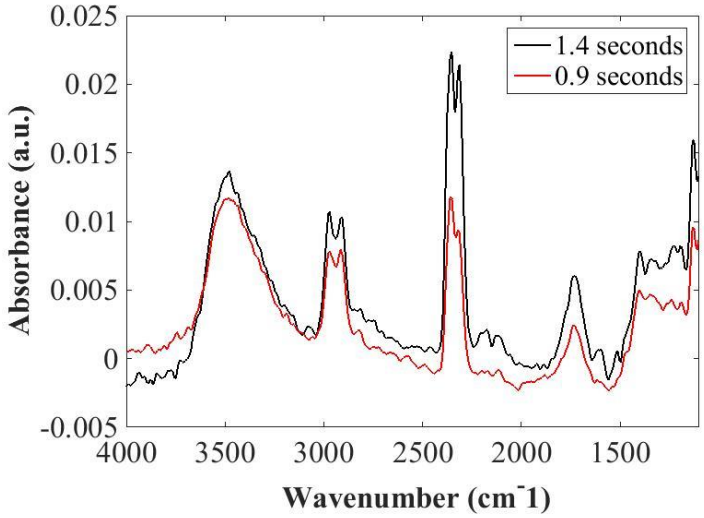

Figure 26. Cellulose pyrolysis spectra at 0.9 and 1.4 s residence times.

When Comparing Figure 11 and 26 (after reactor modification), we can see that the absorbance of the peaks are closer together at different residence times and also the peaks at 1000 and 3500 cm^{-1} are not higher in case of the lower product residence times. One inference could be that the recirculation played a role in increasing the absorbance of those peaks as well as the residue seen on the windows while pyrolyzing cellulose. Taking into account Beer Lambert's law, we see that the absorbance of peaks at lower product residence times as well as higher product residence times have decreased, this proves that the concentration as well as the path length have decreased.

4.4.2 Lignin Tests

In comparison, Figures 12 and 27 show little difference. Except for the peaks at 3700 cm^{-1}. Also the absorbance of peaks at lower product residence times is shorter in the 1000 to 2000 cm^{-1} compared to that of Figure 12.

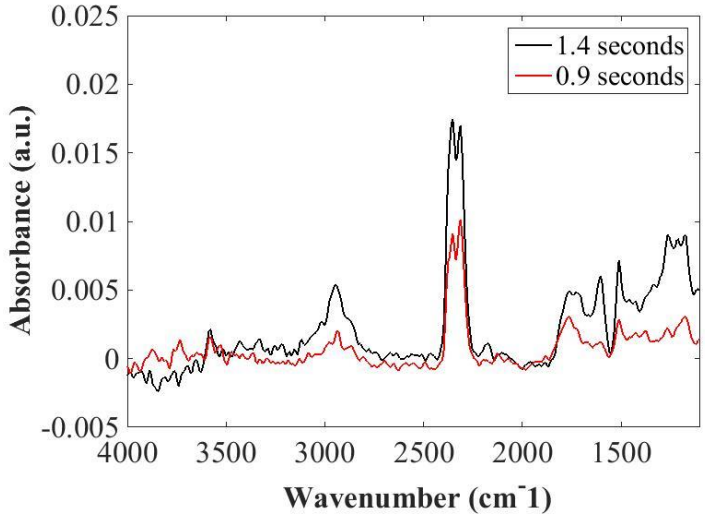

Figure 27 Lignin pyrolysis spectra at 0.9 and 1.4 s residence times

Again we see that the overall absorbance of peaks has reduced, which verifies how concentration as well as change in path length decreases absorbance according to the Beer Lambert law.

4.5 New Reactor Evolution Tests

4.5.1 Cellulose Tests

Figures 28 to 32 show the evolution of products from cellulose pyrolysis at product residence times of 1.4 s.

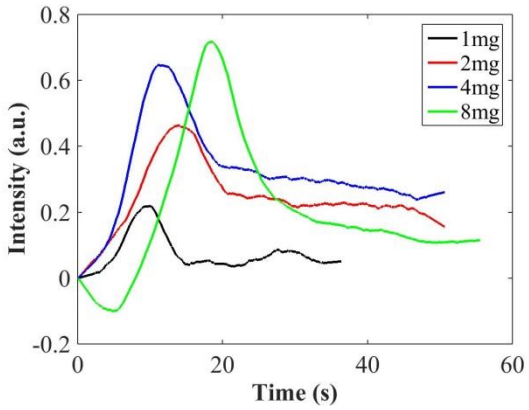

Figure 28. Evolution plots centered around 1720 cm^{-1}.

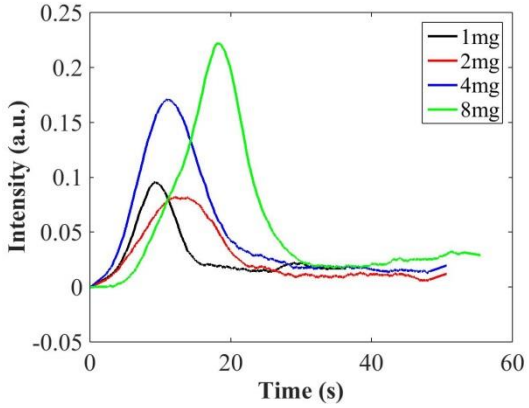

Figure 29. Evolution plots of CO.

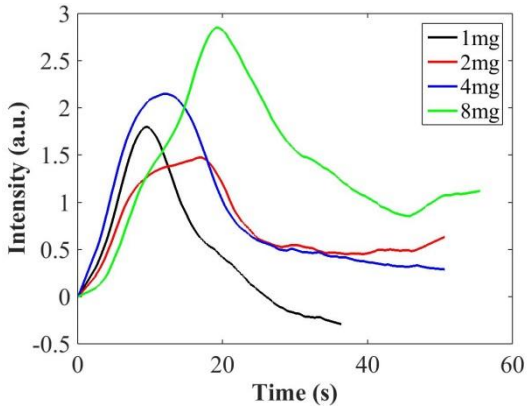

Figure 30. Evolution plots of CO_2.

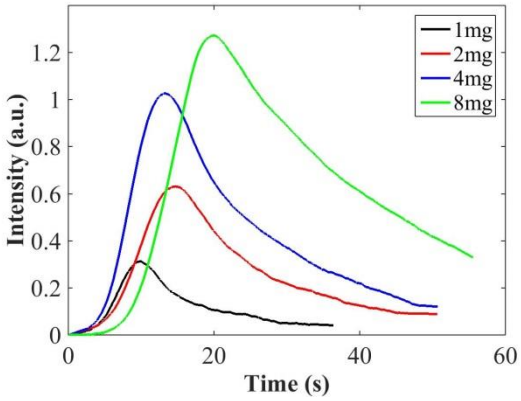

Figure 31. Evolution plots centered around 2940 cm^{-1}.

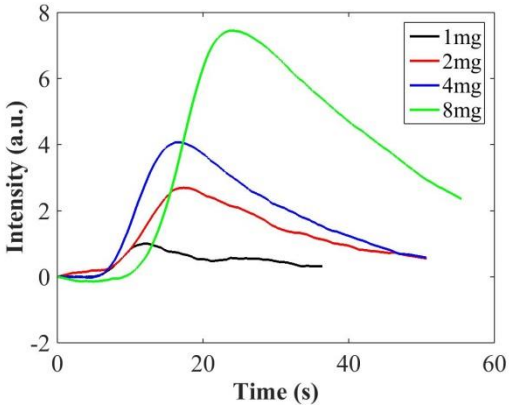

Figure 32. Evolution plots centered around 3430 cm^{-1}.

Figures 32 to 37 show the evolution of cellulose pyrolysis products at lower product residence times of 0.9 seconds.

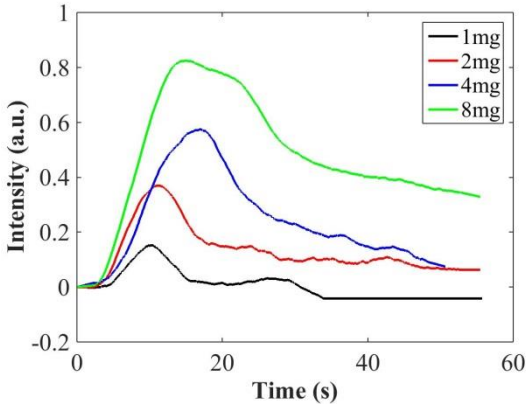

Figure 33. Evolution plots centered around 1720 cm^{-1}.

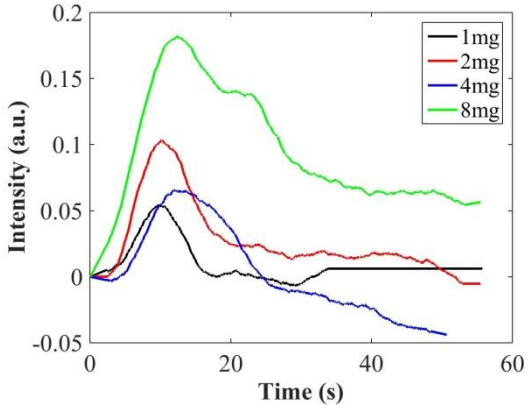

Figure 34. Evolution plots of CO.

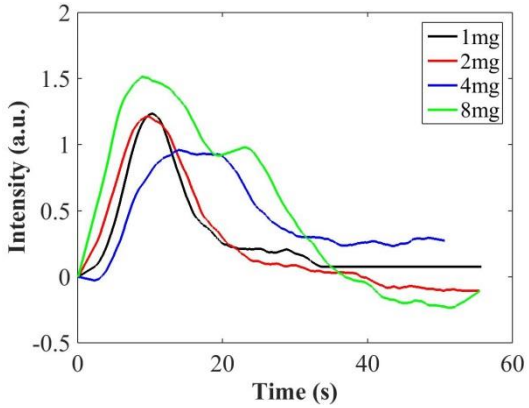

Figure 35. Evolution plots of CO_2.

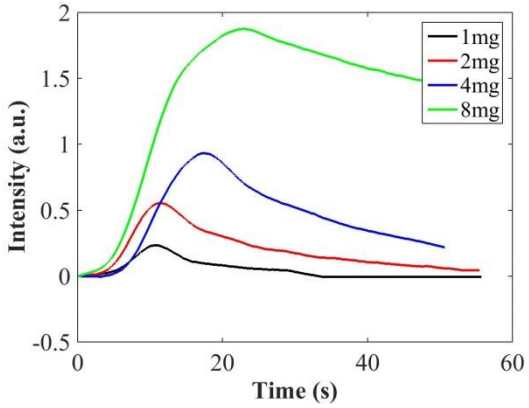

Figure 36. Evolution plots centered around 2940 cm^{-1}.

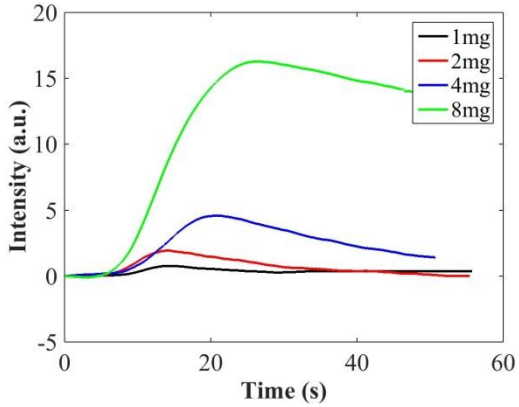

Figure 37. Evolution plots centered around 3430 cm^{-1}.

4.5.2 Lignin Tests

The following Figures 38–41 are the tests of lignin in the new reactor at 1.4 seconds product residence times.

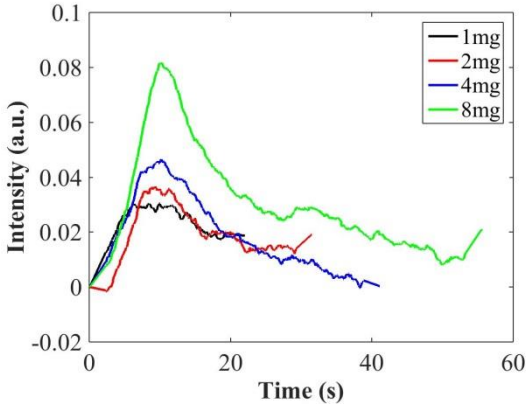

Figure 38. Evolution plots of CO.

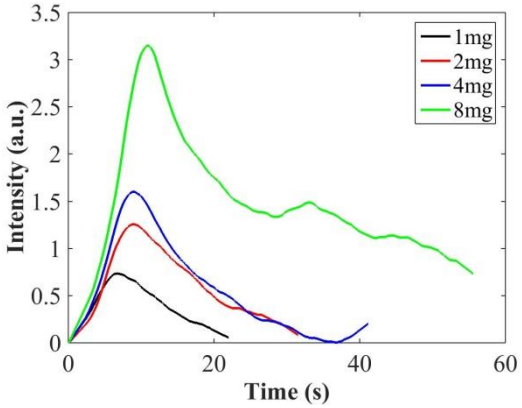

Figure 39. Evolution plots of CO_2.

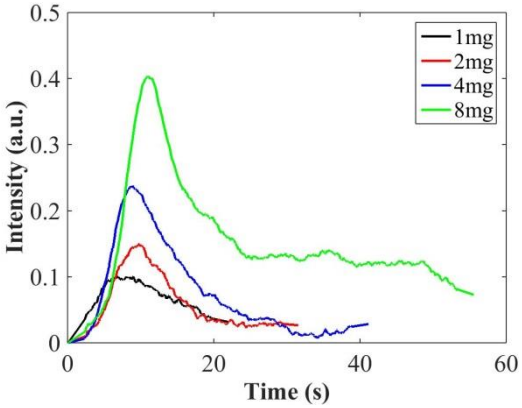

Figure 40. Evolution plots centered around 2940 cm^{-1}.

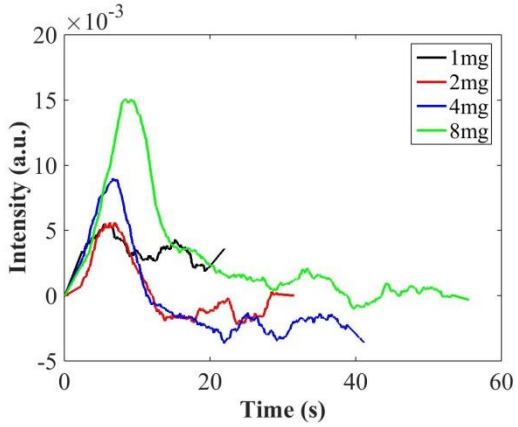

Figure 41. Evolution plots centered around 1747 cm^{-1}.

Figures 42 to 45 are the lignin tests conducted at lower product residence times in the new reactor.

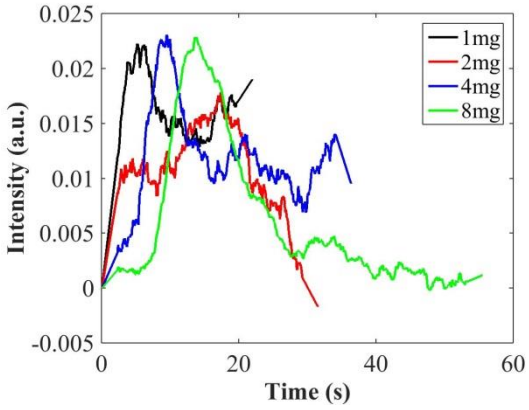

Figure 42. Evolution plots of CO.

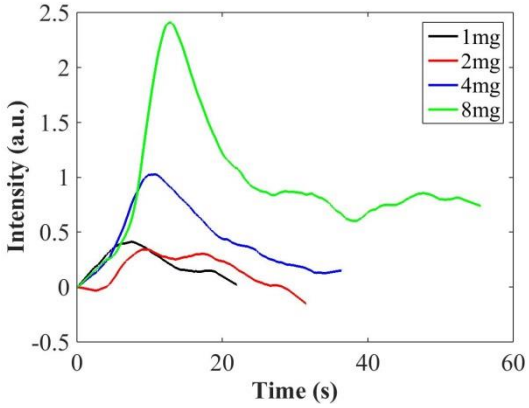

Figure 43. Evolution plots of CO_2.

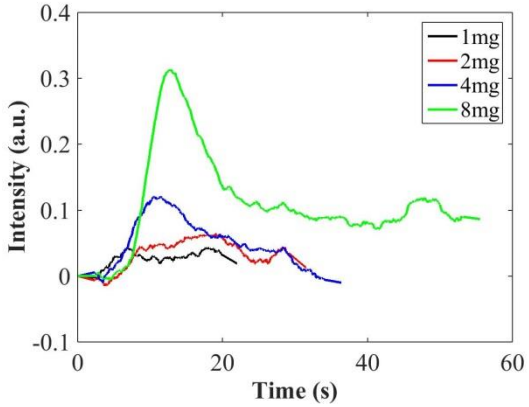

Figure 44. Evolution plots centered around 2940 cm^{-1}.

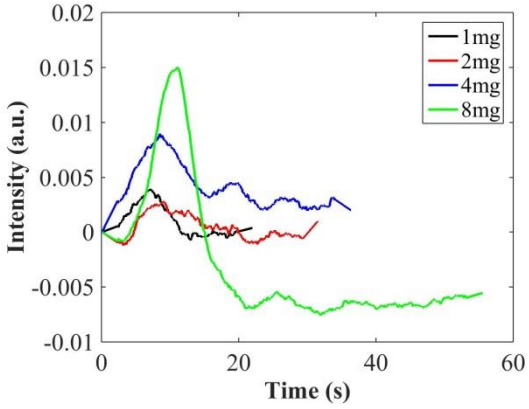

Figure 45. Evolution plots centered around 1747 cm^{-1}.

From the above figures it can be seen that recirculation has been greatly reduced, except in the cases of Figures 41, 43, and 45, which could be due to not allowing the system to purge for longer. However, it should be kept in mind that the windows are not pushed closely to the pyrolysis cavity in the center of the reactor. The intensities of higher mass values of cellulose and lignin do not reach zero. They however show a decreasing trend and it is likely that with higher run times they will reach zero. Again, there are instances of intensities going below zero towards the tail end of plots in the case of Figure 42 of CO. It is possible that since the release of CO is very low compared to other species, there could be poisoning by atmospheric CO, keeping in mind that the IR beam is brought out of the system and passed through the reactor. Even though the system is purged with nitrogen, it is not pure nitrogen, and as we see from the background in Figure 3 there are still impurities in the purge.

From the evolution graphs of cellulose we see that the product with the highest intensity was CO_2, except in the 8 mg case at the higher residence time. From the literature it is confirmed through these plots that the evolution of CO_2 is generally much higher compared to CO in cellulose. Also in comparing the intensities of CO and the intensities of CH stretching CO intensities are higher [9]. However, it must be stated that these studies are conducted in slow pyrolysis conditions.

From the evolution graphs of lignin we see that the product with the highest intensity is also CO_2. In comparing the literature containing TG-FTIR data we see that CO_2 intensities at the peaks are close to 12 times that of the CH(probably methane) stretch peaks [9]. When comparing the data of the new reactor we see that there is a ratio of 7:1

with respect to intensities. This can be attributed to fast pyrolysis and the relatively low yields of gas compared to slow pyrolysis.

4.5.3 Cellulose Product Time Evolution Data

Since the recirculation has been reduced we can now study the times at which different products evolve. Figures 46 and 47 below are plotted by first taking the intensities of different species and normalizing them to 1 and then plotting the rise of the intensities to that maximum. The first set of plots from Figure 46 is taken at residence times of 1.4 s and with cellulose as the sample.

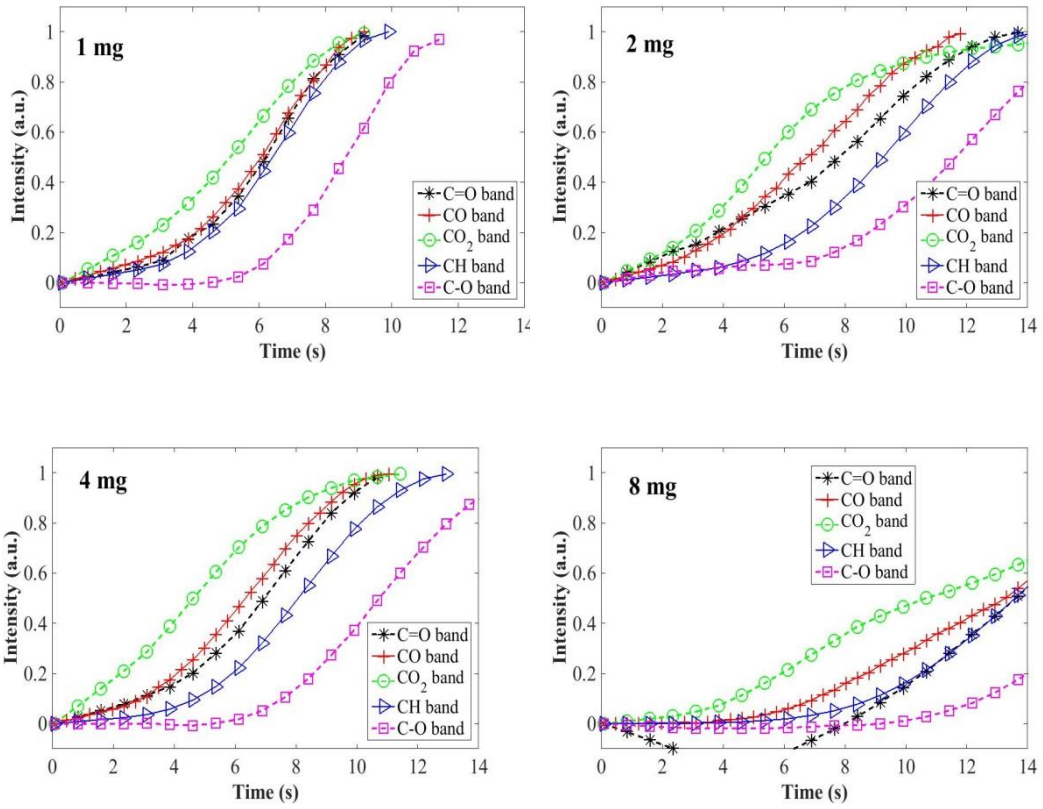

Figure 46. Normalized time-evolution profiles during cellulose pyrolysis at product residence time of 1.4 s.

Figure 47 shows the plots for cellulose pyrolysed at a vapor residence time of 0.9 s.

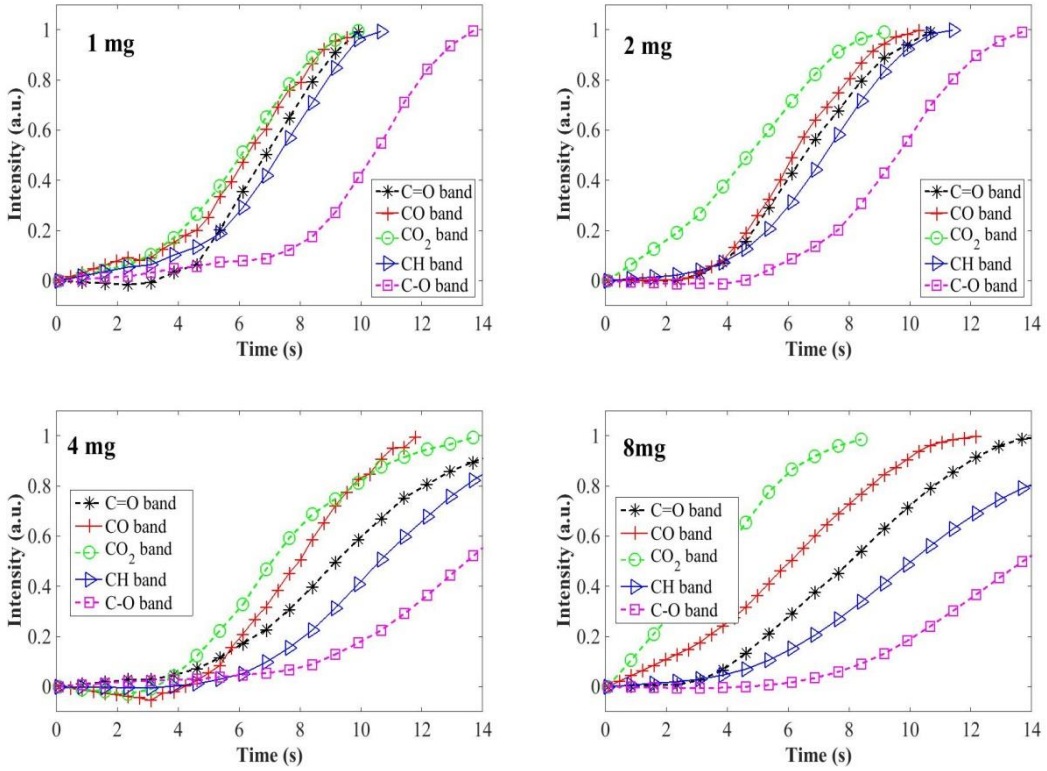

Figure 47. Normalized time-evolution profiles during cellulose pyrolysis at product residence time of 0.9 s.

From Figure 46 we can see that in all cases CO_2 is the first to rise, and in contrast the CH and C-O bands are consistently the last to evolve. The same trend is seen in the case of the higher residence time of 0.9 seconds. To obtain a numerical value for the rise times, the same data was analyzed for time taken for each species to reach 50% of its highest intensity. The values are plotted in Figure 48, which represents the evolution at different mass loading and at a product residence time of 1.4 s. According to literature

CO_2 and water vapor are the first products to form during slow pyrolysis. This is the initial dehydration of the cellulose [9] [25].

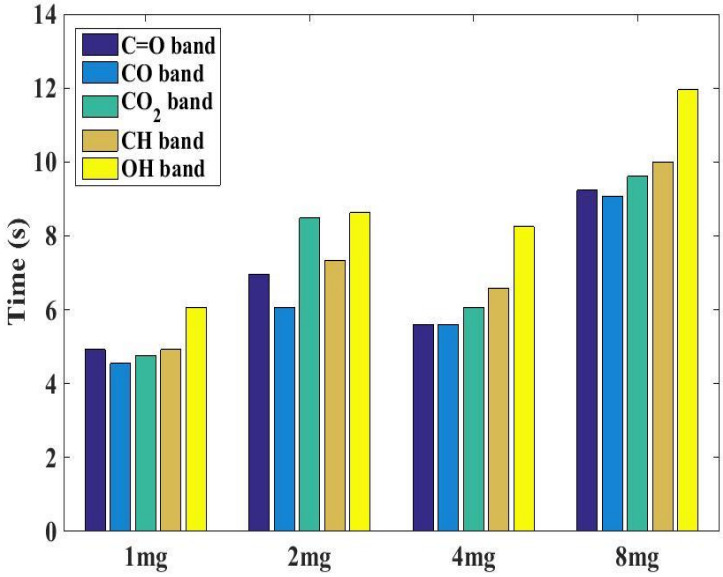

Figure 48. Time evolution of pyrolyzed cellulose species at 50% of their normalized peak intensity at product residence time of 1.4 s.

Contradictory from what is seen in Figure 46 is that CO_2 does not evolve first when considering only 50% of the maximum evolution intensity this again could be due to atmospheric poisoning. However it can be noted that the CH bands and OH stretching bands follow a chronological pattern. This could mean that species like carboxylic acid could be the first to evolve before species like methane or formaldehyde and finally phenols or other compounds that have characteristic absorptions at 3430 cm^{-1}. Figure 49 shows the evolutions of products at product residence times 0.9 s, Again it can be seen that the CH groups and the OH stretching groups are formed at the last and also that the carbonyl band species are formed earlier.

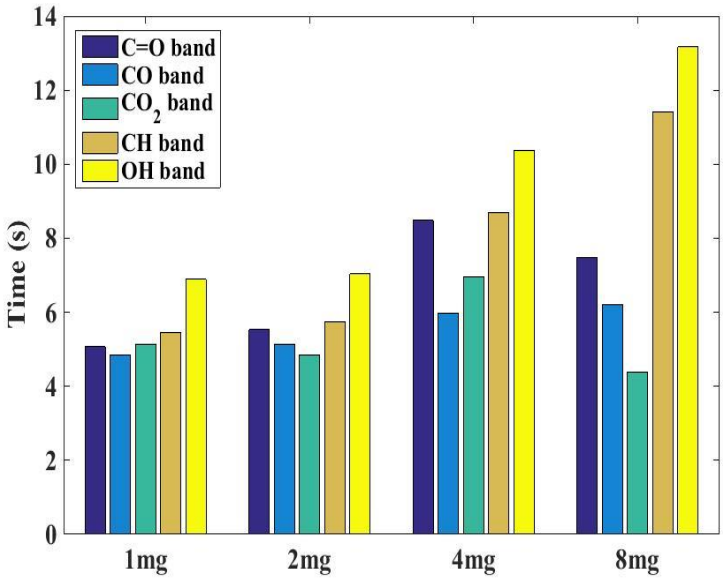

Figure 49. Time evolution of pyrolyzed cellulose species at 50% of their normalized peak intensity at product residence time of 0.9 s.

The above findings for cellulose can be compared with the kinetics model developed by Broadbelt et al. [51]. Based on the kinetics of different glucose reactions that occur after degradation from cellulose, it was determined that products which have C=O band stretches evolve earlier when compared to products in the CH band stretch. This is consistent with the data shown in Fig. 49. Common chemicals that are seen in the fast pyrolysis of cellulose that have these vibrations are formic acid in the case of C=O band stretch and formaldehyde in the case of CH band stretch. Broadbelt et al. [51] determined that formic acid is the result of cyclic Grob fragmentation of β-D-glucofuranose to yield hydroxylallyl ester, which in turn undergoes a retro-aldol reaction to from formic acid. The formation of formaldehyde can take three different routes [51] the first being the C-C bond rupture of 5-hydroxymethylfurfural, the second being the

cyclic Grob fragmentation of β-3-ketohexose, and the third involving the Grob fragmentation of D-glucose [51]. The chemical reaction rate constants for all the pathways were determined using the activation energies and the pre-exponential factors determined experimentally or by quantum chemical calculations by Broadbelt et al [51].

It was also determined that formic acid with a characteristic C=O band stretch is formed before formaldehyde, which has a CH band stretch, provided that formaldehyde evolved by the above-mentioned paths 1 and 3. Although the differences are not dramatic in Fig. 49, this trend appears to be consistent as well with the current experimental results. Keeping temperature and pressure constant the summation of the reaction rates of path 1 and 3 were 0.0057 and 1.0269 x 10^{-5} s^{-1} and that of the formic acid reactions is 0.0148 s^{-1}.

Finally, in comparing the evolution rates of the C=O band products with the current work it was seen to rise with higher mass loadings. Zhou et al. [52] determined that formic acid yield reaches a maximum at 3-4 s, which is shorter than the rise times seen in Figs. 46 and 47. Since the times taken to obtain maximum yield of formic acid increases with each mass loading in the current work, it is possible that this difference is due to heat transfer limitations in the experimental apparatus.

4.5.4 Lignin Product Time Evolution Data

Just like Figures 46 and 47, Figures 50 and 51 have been normalized to 1 and plotted. Figure 50 shows evolution times of pyrolysed lignin at vapor residence time 1.4 seconds.

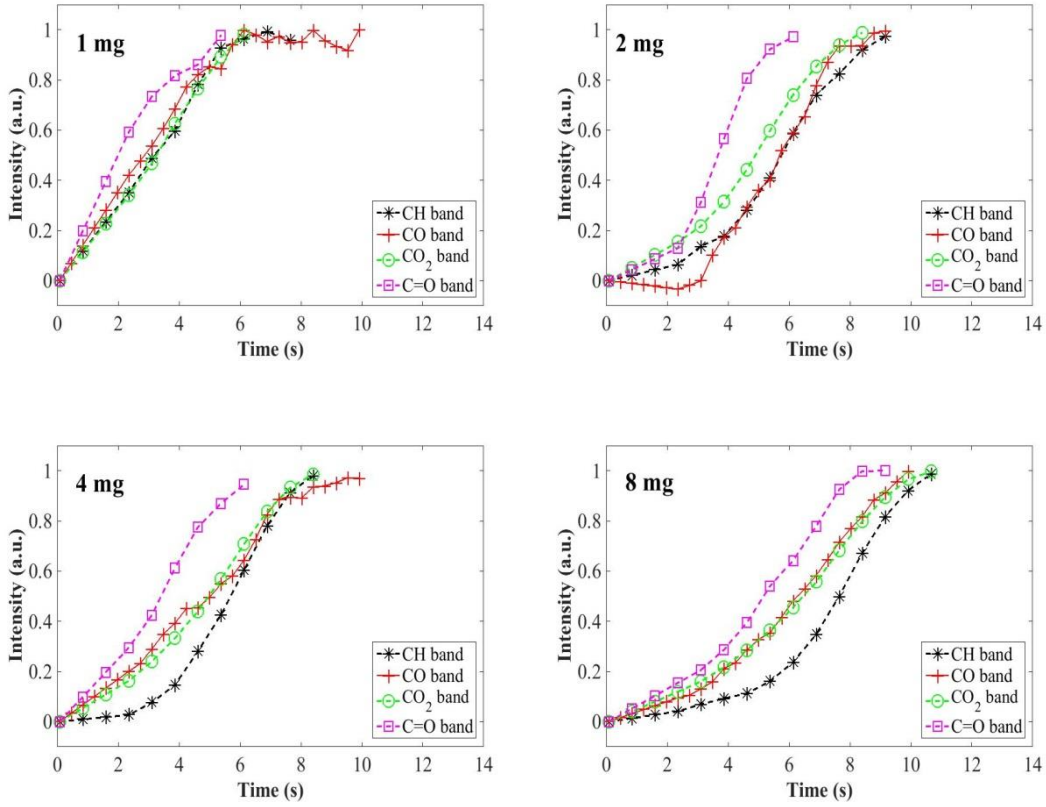

Figure 50. Normalized time-evolution profiles during lignin pyrolysis at product residence time of 1.4 s.

Figure 51 below shows the time evolution of pyrolyzed lignin at a product residence time of 0.9 s.

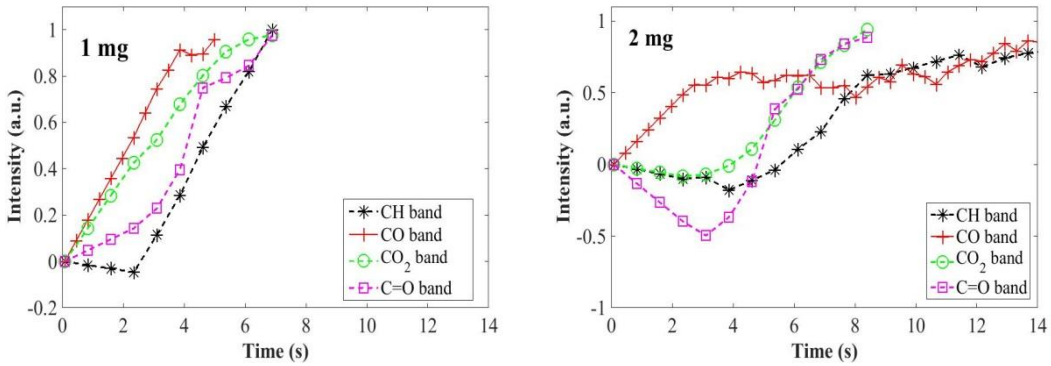

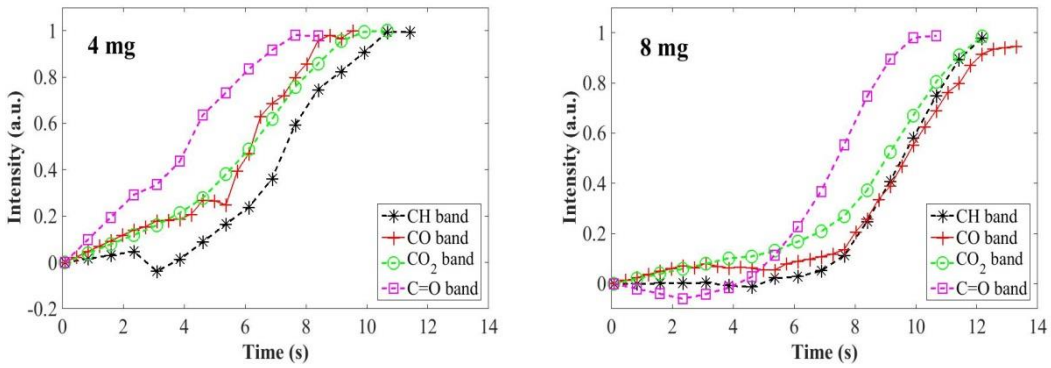

Figure 51. Normalized time-evolution profiles during lignin pyrolysis at a product residence time of 0.9 s.

In comparing Figures 49 and 51, we see that the carbonyl groups are first to evolve, then followed by the methoxyl group species. Only in the cases of 1 mg and 2 mg at 0.9 seconds product residence time do we see that this is not the case. In the 1 mg case, it is possible that the CO and CO_2 intensities were contaminated by atmospheric CO and CO_2. In the 2 mg case it can be seen that there was a lot of recirculation probably due to the system having insufficient time to purge between tests. However one can assume that if the plot is corrected that the carbonyl slope will be the first to reach the normalized peak value.

To compare the evolution times of species, data on rise times were plotted to show the various bands and respective evolution times at different mass loadings. Figures 52 and 53 show the time-evolution of products taken at the point where they reach 50% of the normalized intensity at product residence times of 1.4 and 0.9 s, respectively.

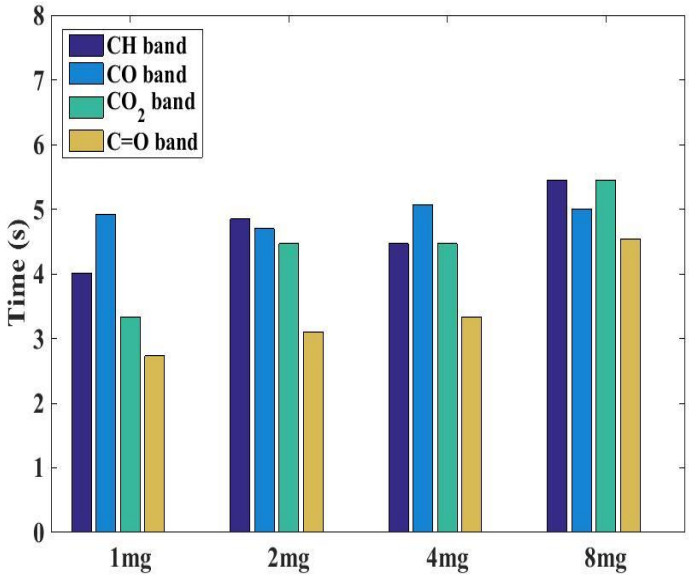

Figure 52. Time evolution of pyrolyzed lignin species at 50% of their normalized peak intensity at product residence times of 1.4 s.

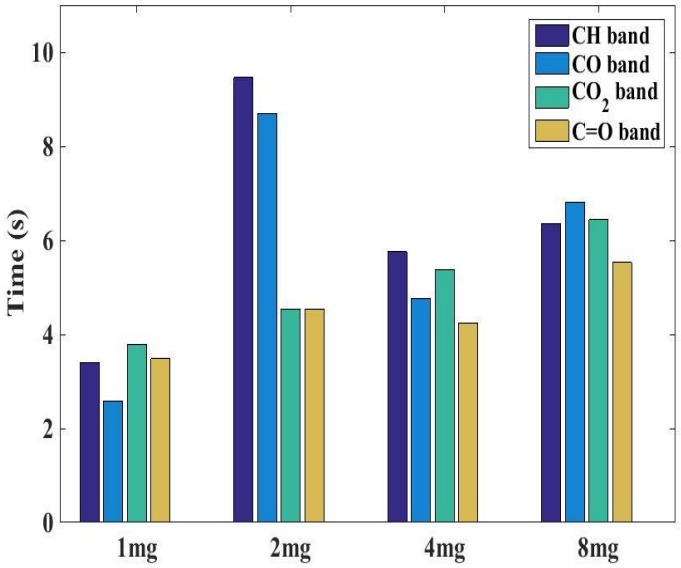

Figure 53. Time evolution of pyrolyzed lignin species at 50% of their normalized peak intensity at product residence times of 0.9 s.

When considering only the carbonyl band species and the CH band species we see that the species associated with carbonyl band absorption are the first to evolve in both the case of both product residence times. This could mean that in the fast pyrolysis of lignin at residence times of 1.4 and 0.9 s, species belonging to the carbonyl group evolve first before the species in the CH group.

CHAPTER 5. CONCLUSIONS AND RECOMMENDATIONS

5.1 General Conclusions

A bench scale pyrolysis reactor with *in-situ* measurement capability was designed and fabricated. Cell characterization was performed to obtain the reaction temperatures required to represent fast pyrolysis conditions. Fourier Transform Infrared (FTIR) spectroscopy was used as a tool to study the time dynamics of fast pyrolysis. In order to conduct the study changes to the original FTIR experimental set up were needed reduce the effects of product recirculation within the cell and obtain meaning time evolution data. A sample insertion mechanism was developed to allow the biomass to be rapidly introduced to the high-temperature atmosphere. Cellulose and Lignin were chosen as the experimental samples for studies. Data was obtained on the kinetics of the pyrolysis of these materials. Two product residence times were studied, including 0.9 and 1.4 s. The time-evolution data for these two samples were studied at the two residence times and the following conclusions were obtained.

1. In the fast pyrolysis of cellulose at product residence times of 0.9 and 1.4 s, the carbonyl compounds evolve before the CH band compounds, followed by hydroxide compounds.
2. In the fast pyrolysis of lignin at product residence times of 0.9 and 1.4 ss, the carbonyl containing compounds evolve before the CH band compounds.

5.2 Recommendations

Recirculation of product gases was greatly reduced in the current cell, but was not completely eliminated. This was seen in the later tests after modification of the reactor to move the windows closer to the pyrolysis cavity. A reactor with windows even closer to the pyrolysis cavity would reduce the recirculation even further. To reduce the possibility of contamination in the FTIR spectra, ultra-pure purge gas should be used along the FTIR beam path. A heater should be used that is not a coil, as it causes problems in the computational analysis of the reactor. Instead of a custom-made gas heater, a more controllable heater should be used to maintain the temperature of the sweep gas. This will allow for better characterization of the reactor. A mechanized sample insertion should be developed as this can be used to study the exact time difference between different experiments and, therefore, of species evolutions based on different operating parameters (e.g., temperature, mass loadings, etc.). Finally, additional effort, perhaps including higher precision machining, should be made to reduce any potential leaks in the system.

REFERENCES

[1] World Energy Council, "World Energy Trilemma," 2013.

[2] US Department of energy, "Clean cities Alternative Fuel Price Report," 2014.

[3] Javaid Akhtar and NorAishah Saidina Amin "A Review on Operating parameters for Optimum Liquid Oil Yield in Biomass Pyrolysis" *Renewable and Sustainable Energy Reviews*, vol. 16, no. 7, pp. 5101-5109, 2012.

[4] Mi-Kyung Bahng, Calvin Mukarakate, David J. Robichaud, and Mark R. Nimlos "Current technologies for analysis of biomass thermochemical processing: A review" *Analytica Chimica Acta*, vol. 651, no. 2, pp. 117-124, 2009.

[5] Mohammad I. Jahirul, Mohammad G. Rasul, Ashfaque Ahmed Chowdhury, Nanjappa Ashwath, and "Biofuels production through Biomass Pyrolysis- A Technological Review," *Energies*, vol. 5, pp. 4952-5001, 2012.

[6] Dinesh Mohan, Charles U.Pittman and Philip H.Steele "Pyrolysis of wood/ biomass for bio oil : A critical review" *Energy Fuels*, vol. 20, no. 3, pp. 849-889, 2005.

[7] Dr. Samy Sadak, "Pyrolysis",http://bioweb.sungrant.org/NR/rdonlyres/57BCB4D0-1F59-4BC3-A4DD-4B72E9A3DA30/0/Pyrolysis.pdf, pp. 1-24.

[8] K.Raveendran, Anuradda Ganesh, and Kartic C.Khilart "Influence of Mineral Matter on Biomass Pyrolysis Characteristics" *Fuel*, vol. 74, no. 12, pp. 1812-1822, 1995.

[9] Haiping Yang, Rong Yan, Hanping Chen, Dong Ho Lee and Chuguang Zheng "Characteristics of hemicellulose, cellulose and lignin pyrolysis" *Fuel*, vol. 86, no. 12-13, pp. 1781-1788, 2006.

[10] R.Bassilakis, R.M. Carangelo and M.A.Wojtowicz "TG-FTIR analysis of biomass pyrolysis" *Fuel*, vol. 80, no. 12, pp. 1765-1786, 2001.

[11] A.V.Bridgwater, "Review of Fast Pyrolysis of Biomass and Product Upgrading" *Biomass and Bioenergy*, vol. 38, pp. 68-94, 2012.

[12] Ayhan Demirbas and Gonenc Arin, "An Overview of Biomass Pyrolysis" *Energy Sources*, vol. 24, pp. 471-482, 2002.

[13] Pushkaraj R.Patwardhan, Justinus A.Satrio, Robert C. Brown and Brent H. Shanks "Product distribution from fast Pyrolysis fo Glucose based Carbohydrates" *Journal of Analytical and Applied Pyrolysis*, vol. 86, no. 2, pp. 323-330, 2009.

[14] A.V. Bridgwater, D.Meier and D.Radlein "An overview of fast pyrolysis of biomass" *Organic Geochemisry*, vol. 30, no. 12, pp. 1479-1493, 1999.

[15] John E. White, W.James Catallo and Benjamin L.Lengendre "Biomass pyrolysis kinetics: A comparative critic review with relevant agricultural residue cases" *Journal of analytical and applied pyrolysis*, vol. 91, no. 1, pp. 1-33, 2011.

[16] T. Harding E.Salehi and J. Abedi "Bio-oil from Sawdust: Pyrolysis of Sawdust in a fixed bed system" *Energy and fuels*, vol. 23, pp. 3767-3772, 2009.

[17] Mohamad Azri Sukiran, Chow Mee Chin and Nor Kartini Abu Bakar "Bio-oils from Pyrolysis of Oil Palm Empty Bunches," *American Journal of Applied Sciences*, vol. 6, no. 5, pp. 869-875, 2009.

[18] Hasan Ferdi Gercel "The Effect of a Sweeping Gas Flow Rate on the Fast Pyrolysis of Biomass" *Energy Sources*, vol. 24, pp. 633-642, 2002.

[19] Wan Nor Roslam Wan Isahak, Mohamed W.M.Hisham, Mohd Ambar Yarmo and Taufiq-yap Yun Hin "A Review on Bio oil Production from Biomass by Using Pyrolysis Method" *Renewable and Sustainable Energy Reviews*, vol. 16, no. 8, pp. 5910-5923, 2012.

[20] M. Nik-Azar, M.R. Hajaligol, M.Sohrabi and B.Dabir "Mineral matter effects in rapid pyrolysis of beech wood" *Fuel Processing Technology*, vol. 51, no. 1-2, pp. 7-17, 1997.

[21] Scott D.S., Majerski P, Piskorz J, Radlein D. "A Second Lookat Fast Pyrolysis of Biomass-the RTI Process" *Journal of analytical and applied pyrolysis* , pp. 23-37, 1999.

[22] Aylo'n E., Ferna'ndez Colino A, Navarro M.V., Murillo R, Garci'a T,Mastral AM "Waste tyre Pyrolysis: Comparison of fixed bed and moving bed reactor" *Industrial And Engineering Chemistry Research*, vol. 47, pp. 4029-4033, 2008.

[23] H.S. Gulbaran Tulbentci and Sai Yorgun "Pyrolysis of Sunflower Press Bagasse: Heating Values and Energy Distribution of the Pyrolysis Products" *Energy Sources*, vol. 25, pp. 809-817, 2003.

[24] Francois Xavier Collard and Joel Blin "A Review on Pyrolysis of Biomass constituents: MEchanisms and composition of the products obtained from conversion of cellulose, hemicellulose and lignin" *Renewable and Sustainable Energy Reviews*, vol. 38, pp. 594-608, 2014.

[25] F. Shafizadeh, "Introduction to Pyrolysis" *Journal of analytical and applied pyrolysis*, pp. 283-305, 1982.

[26] Dennis Y.C. Leung, X.L. Yin, and C.Z. Wu "a review of the development and commercialiaztion of biomass gasification Technologies in China" *Renewable and Sustainable Energy Reviews*, vol. 8, no. 6, pp. 565-580, 2004.

[27] B.M. Wagenaar, W.Prins and W.P.M. Van Swaaij "Pyrolysis of Biomass in the Rotating Cone Reactor: Modelling and Experimental Justification" *Chemical Engineering Science*, vol. 49, no. 24, pp. 5109-5126, 1994.

[28] A. Veses, M. Aznar, I. Martinez, J.D. Martinez, J.M. Lopez and M.V. Navarro "Catalytic Pyrolysis of Wood Biomass in an Auger Reactor Using Calcium-Based Catalysts" *Bioresource Technology*, vol. 162, pp. 250-258, 2014.

[29] Capucine Dupont, Jean -Micahel Commandre, Paola Gauthier, Guillame Boissonnet, Sylvain Salvador, Daniel Schweich "Biomass Pyrolysis Experiments in an Analytical Entrained Flow Reactor between 1073K and 1273 K" *Fuel*, vol. 87, no. 7, pp. 1155-1164, 2007.

[30] L.Tang, H.Huang, H.Hao and K.Zhao "Development of Plasma Pyrolysis/Gasification Systems for Energy Efficient and Envieronmentally Sound Waste Disposal" *Journal of Electrostatics*, vol. 71, no. 5, pp. 839-847, 2013.

[31] Xiqiang Zhao, Min Wang, Hongzhen Liu, Longzhi Li, Chunyuan Ma and Zhanlong Song "A microwave reactor for characterization of pyrolyzed biomass" *Biosource Technology*, vol. 104, pp. 673-678, 2012.

[32] Su Shiung Lam, Alan D. Russell, Howard A Chase "Microwave Pyrolysis, a Novel Process for Recycling Waste Automotive Engine Oil" *Energy*, pp. 2985-2991, 2010.

[33] Sergio Morales, Rosa Miranda, Diana Bustos, Thania Cazares, Honghi Tran "Solar biomass pyrolysis for the production of bio-fuels andchemical commodities" *Journal of Analytical and Applied Pyrolysis*, pp. 65-78, 2014.

[34] Jani Lehto, Anja Oasmaa, Yrjö Solantausta, Matti Kytö and David Chiaramonti "Review of fuel oil quality and combustion of fast pyrolysis bio-oils from lignocellulosic biomass" *Applied Energy*, vol. 116, pp. 178-190, 2014.

[35] Pankaj K. Kanaujia, Y.K. Sharma, M.O. Garg, Deependra Tripathi and Raghuvir Singh "Review of analytical strategies in the production and upgrading of bio-oils derived from lignocellulosic biomass" *Journal of Analytical and Applied Pyrolysis*, vol. 105, pp. 55-74, 2014.

[36] Barbara Stuart, *Infrared Spectroscopy: Fundamentals and Applications*.: Wiley, 2004.

[37] P.S. Mcintyre W.O. George, *Infrared Spetroscopy*.: John Wiley & Sons, 1987.

[38] B.C Smith, *Fundamentals of Fourier transform Infrared Spectroscopy*.: Taylor and Francis Group, 2011.

[39] John Coates, "Interpretation of Infrared Spectra, A practical Appraoch" *Encyclopedia of Analytical Chemistry*, 2000.

[40] Mark C. Abrams, James W. Brault Sumner P.Davis, *Fourier Transform Spectrometry*.: Academic Press, 2001.

[41] Robert White, *Chromatography/Fourier Transform Infrared Spectroscopy and its Applications*.: Marcel Decker, 1990.

[42] Xiaoxiang Jiang, Naoko Ellis, Dekui Shen, Jianchun Jiang, Weidi Dai and Zhaping Zhong "Thermogravimetric- FTIR analysis of pyrolysis of pyrolytic lignin extracted from bio-oil" *Chemical Engineering and Technology*, vol. 35, no. 5, pp. 827-833, 2011.

[43] S.Li, J.Lyons-Hart, J.banyasz and K.Shafer "Real-Time evolved gas analysis by FTIR method: an experimental study of cellulose pyrolysis" *Fuel*, vol. 80, no. 12, pp. 1809-1817, 2001.

[44] T.Siengchum, Mathew Isenberg, Steven S.C.Chuang "Fast Pyrolysis of coconut biomass- An FTIR study" *Fuel*, pp. 559-565, 2013.

[45] Qian Liu, Shurong Wang, Yun Zheng, Zhongyang Luo and Kefa Cen "Mechanism study of wood lignin pyrolysis by using TG-FTIR analysis" *Journal of Analytical and Applied Pyrolysis*, vol. 82, no. 1, pp. 170-177, 2008.

[46] Hui Zhou, AiHong Meng, YanQiu Long, QingHai Li and YanGuo Zhang "Interactions of municipal solid waste components during pyrolysis- a TG-FTIR study" *Journal of Analytical and Applied Pyrolysis*, vol. 108, pp. 19-25, 2014.

[47] Luo Supeng, Bao Guirong, Wang Hua, Li Fashe and Li Yizhe "TG-DSC-FTIR analysis of cyanobacteria pyrolysis" *Physics Procedia*, vol. 33, pp. 657-662, 2012.

[48] Peng Fu, Song Hu, Jun Xiang, Peisheng Li, Dan Huang , Long Jiang, Anchao Zhang and Junying Zhang "FTIR study of pyrolysis products evolving from typical agricultural residues" *Journal of Analytical and Applied Pyrolysis*, vol. 88, no. 2, pp. 117-123, 2010.

[49] Seong-Beom Lee and Oladiran Fasina "TG-FTIR of switchgrass pyrolysis" *Journal of Analytical and Applied Pyrolysis*, pp. 39-43, 2009.

[50] Wang Shurong, Liu Qian, Luo Zhongyang, Wen Lihua, Cen Kefa "Mechanism study on cellulose pyrolysis using thermogravimetric analysis coupled with infrared spectroscopy" *Frontiers in Energy* , vol. 1, no. 4, pp. 413-419, 2007.

[51] R. Vinu and Linda J. Broadbelt, "A mechanistic model of fast pyrolysis of glucose-based carbohydrates to predict bio-oil composition" *Energy and Environmental Science*, vol. 5, no. 12, pp. 9808-9826, 2012.

[52] Michael W. Nolte, Heather B. Mayes, Brent H. Shanks and Linda J. Broadbelt Xiaowei Zhou, "Experimental and mechanistic modeling of fast pyrolysis of neat glucose-based carbohydrates. 1. Experiments and development of a detailed mechanistic model" *Industrial and Engineering Chemistry Research*, vol. 53, no. 34, pp. 13274-13289, 2014.

APPENDIX A. DATA FILTERING

While calculating the evolution data, the graphs showed high frequency noise. To curb this problem they were all filtered using the Savitzky Golay function in Matlab. The figure below is an example of the filtering. It is the evolution of CO at vapor residence time 0.9 s from the pyrolysis of 1mg of cellulose.

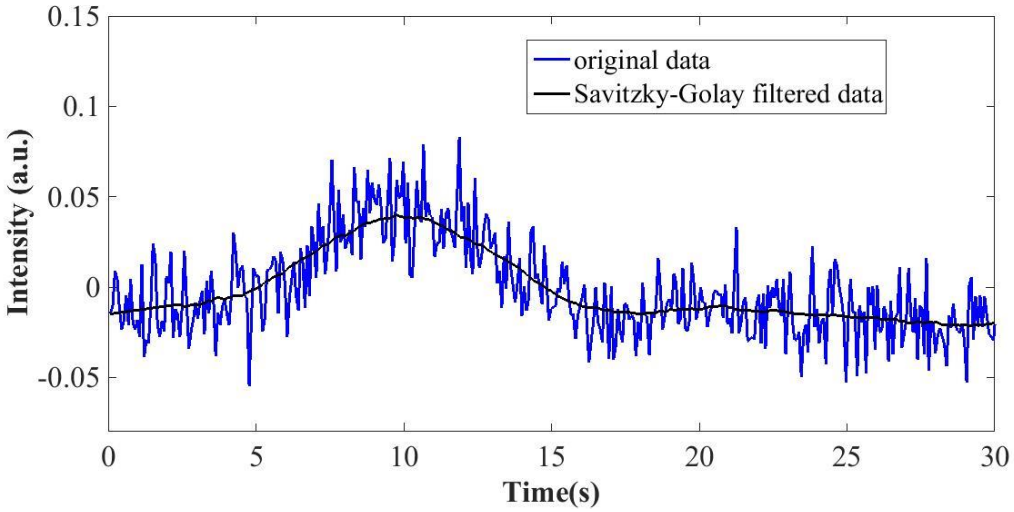

APPENDIX B. SAMPLE SPECTRA

Below are the plots obtained by the pyrolysis of phenol, biphenol and red oak at product residence times of 1.4 s.